RESEARCH ARTICLE

A Single-Cell Taxonomy Predicts Inflammatory Niche Remodeling to Drive Tissue Failure and Outcome in Human AML

Lanpeng Chen, Eline Pronk, Claire van Dijk, Yujie Bian, Jacqueline Feyen, Tim van Tienhoven, Meltem Yildirim, Paola Pisterzi, Madelon M.E. de Jong, Alejandro Bastidas, Remco M. Hoogenboezem, Chiel Wevers, Eric M. Bindels, Bob Löwenberg, Tom Cupedo, Mathijs A. Sanders, and Marc H.G.P. Raaijmakers

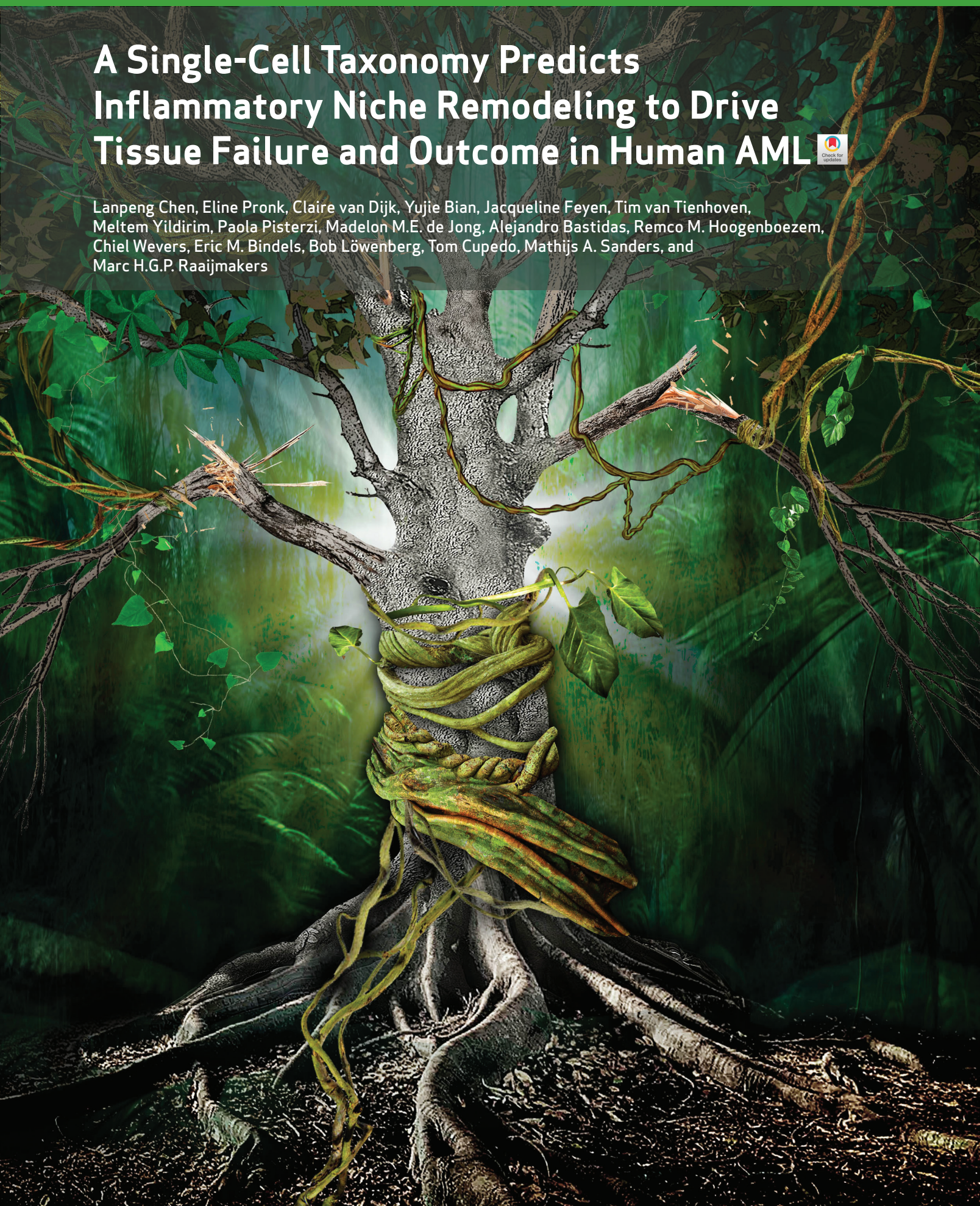

ABSTRACT Cancer initiation is orchestrated by an interplay between tumor-initiating cells and their stromal/immune environment. Here, by adapted single-cell RNA sequencing, we decipher the predicted signaling between tissue-resident hematopoietic stem/progenitor cells (HSPC) and their neoplastic counterparts with their native niches in the human bone marrow. LEPR$^+$ stromal cells are identified as central regulators of hematopoiesis through predicted interactions with all cells in the marrow. Inflammatory niche remodeling and the resulting deprivation of critical HSPC regulatory factors are predicted to repress high-output hematopoietic stem cell subsets in *NPM1*-mutated acute myeloid leukemia (AML), with relative resistance of clonal cells. Stromal gene signatures reflective of niche remodeling are associated with reduced relapse rates and favorable outcomes after chemotherapy across all genetic risk categories. Elucidation of the intercellular signaling defining human AML, thus, predicts that inflammatory remodeling of stem cell niches drives tissue repression and clonal selection but may pose a vulnerability for relapse-initiating cells in the context of chemotherapeutic treatment.

SIGNIFICANCE: Tumor-promoting inflammation is considered an enabling characteristic of tumorigenesis, but mechanisms remain incompletely understood. By deciphering the predicted signaling between tissue-resident stem cells and their neoplastic counterparts with their environment, we identify inflammatory remodeling of stromal niches as a determinant of normal tissue repression and clinical outcomes in human AML.

See related commentary by Lisi-Vega and Méndez-Ferrer, p. 349.

INTRODUCTION

Cancer initiation and drug resistance are orchestrated by an interplay between tumor-initiating cells, residual normal tissue stem and progenitor cells, and ancillary tissue-resident cells, comprising the stromal and immune environment (1). Ultimately, insight into the signaling cascades operative between all these cells in a neoplastic state is required to obtain a comprehensive appreciation of the complexity of tumorigenesis and tumor survival in the context of therapy.

One important component of all human tissues are stromal cells. Bone marrow stromal cells (BMSC) pervade the tissue in extensive networks that are estimated to comprise up to 20% of the marrow's cellular volume and associate with the vast majority of hematopoietic cells (2). They represent a likely heterogeneous population of cells, with a subset considered critical for the maintenance and homeostatic regulation of hematopoietic stem/progenitor cells (HSPC; ref. 3). A subset of stromal cells comprising the HSPC niche has been characterized in mice by expression of the leptin receptor (LEPR; refs. 4, 5) and high expression of CXCL12 [hence dubbed "CXCL12-abundant reticular (CAR) cells"; refs. 6, 7] located in the vicinity of sinusoid vessels (2, 5, 8). These stromal cells are major sources of stem cell factor (SCF) and interleukin-7 and are considered critical regulators of hematopoietic stem cells (HSC), multipotent progenitors, lymphoid progenitors as well as natural killer (NK), B and plasmacytoid dendritic cell (DC) development (4, 9–12).

It is, however, important to emphasize that these insights have been derived mostly from genetic studies in nonhuman species, particularly mice. The biology, heterogeneity, and interactions of LEPR$^+$ stromal cells in the human bone marrow (BM) have remained largely elusive, in part because it is difficult to retrieve these cells in sufficient numbers, likely because they reside along fibers of the extracellular matrix, limiting their capture by aspiration.

Insight into the biology of human LEPR$^+$ stromal cells, and in particular their interaction with HSPCs, is of likely further relevance to the biology of myeloid neoplasms, including acute myeloid leukemia (AML). AML is caused by genetic events occurring in HSPCs, but mouse modeling and humanized *ex vivo* modeling have implicated stromal niche alterations in the initiation, maintenance, drug resistance, and progression of AML (13–23). Transcriptional alterations in *Lepr*$^+$ stromal cells, including the downregulation of hematopoietic regulatory factors, have further been documented in mice transplanted with MLL-AF9 leukemic cells, suggesting that a leukemic state may attenuate the supportive function of *Lepr*$^+$ stromal cells for normal hematopoiesis (24).

The relevance of these proposed concepts and mechanisms for human disease have, however, remained uncertain, primarily because we lack comprehensive insights on LEPR$^+$ BMSCs in the human leukemic marrow and their potential pathologic interaction with hematopoietic elements.

Here, we performed comprehensive, paired, single-cell transcriptional sequencing and networking analyses of all cells in human normal bone marrow (NBM) and AML aspirates.

The data establish a comprehensive taxonomy of the predicted cellular interactions between LEPR$^+$ stromal niches,

Department of Hematology, Erasmus MC Cancer Institute, Rotterdam, the Netherlands.

Corresponding Author: Marc H.G.P. Raaijmakers, Department of Hematology, Erasmus MC Cancer Institute, Dr. Molewaterplein 40, 3015 GD Rotterdam, the Netherlands. Phone: 31-107043756; E-mail: m.h.g.raaijmakers@erasmusmc.nl

Blood Cancer Discov 2023;4:394–417

doi: 10.1158/2643-3230.BCD-23-0043

HSPCs, and adaptive and innate immune cells in the human NBM and the disruption of these signaling pathways defining AML. Induced deterioration of stromal niche support in AML through inflammatory activation of LEPR$^+$ cells is predicted to broadly affect tissue signaling and induce repression of normal hematopoiesis via disruption of signaling toward high-output HSCs and committed progenitors but is ultimately associated with a favorable prognosis. The data provide human disease relevance to previous findings in model systems and provide a resource of intercellular signaling in the human BM defining native and neoplastic hematopoiesis, with a particular emphasis on the communication between HSPCs and their stromal niches.

RESULTS

A Cellular Taxonomy of the Human NBM

To generate a cellular taxonomy of the human NBM, representing both rare HSPCs and stromal niche populations, allowing assessment of their cellular diversity, and predicted intercellular signaling, we performed single-cell RNA sequencing (scRNA-seq) on viably frozen BM aspirates from four healthy donors for allogeneic transplantation (median age 51; range, 47–53 years; Supplementary Table S1). To ensure a robust representation of all BM cell types in the dataset (enabling accurate assessment of population heterogeneity at high resolution), we used flow cytometry to sort and purify all cells in the aspirates into five fractions: the nonhematopoietic stromal (CD45$^-$CD235a$^-$CD71$^-$CD31$^-$) and nonstromal/endothelial (CD45$^-$CD235a$^-$CD71$^-$CD31$^+$) fraction, the HSPC fraction (CD45$^+$CD34$^+$), the myeloid fraction (CD45$^+$CD34$^-$CD117$^+$/CD33$^+$), and the nonmyeloid (lymphoid) fraction (CD45$^+$CD34$^-$CD117$^-$CD33$^-$; Supplementary Fig. S1A). Fractions were combined into two pools (HSPC with myeloid and nonhematopoietic with nonmyeloid) and subjected to scRNA-seq in separate runs, and the data of the two separate runs were subsequently merged into a single scRNA-seq dataset (Supplementary Fig. S1A).

We acquired high-quality data from 46,740 NBM cells. The purification strategy resulted in a robust representation of low-frequency cell populations such as nonhematopoietic stromal cells and HSCs in the dataset (Fig. 1A).

Using Clustifyr, a package to classify cells from scRNA-seq data using external references (25), the sequenced cells were classified into BMSCs, endothelial cells (EC), CD34$^+$ HSPCs, erythroid progenitors, megakaryocytes (MK), DCs, CD14$^+$ monocytes (CD14$^+$ Mono), CD16$^+$ monocytes (CD16$^+$ Mono), NK cells, CD4$^+$ T cells (CD4 T), CD8$^+$ T cells (CD8 T), B cells (B), and plasma cells (Supplementary Fig. S1B). The accuracy of the unsupervised cell annotation was validated by checking the expression of canonical markers for each cell type (Fig. 1B; Supplementary Fig. S1C and S1D). The BMSC cluster, for instance, specifically expressed BMSC markers *NGFR* (CD271), *PRRX1*, the perivascular MSC marker *LEPR* and the HSPC niche factors *CXCL12* and *KITLG* (Fig. 1B; Supplementary Fig. S1C and S1D). The HSPC cluster expressed *CD34*, *AVP* (26), and *KIT* (Fig. 1B; Supplementary Fig. S1C and S1D) and the CD4$^+$ T, CD8$^+$ T, and NK clusters had enhanced expression of *CD3D*, *CD8B*, and *NKG7*, respectively (Fig. 1B; Supplementary Fig. S1C and S1D).

To dissect the cellular heterogeneity within the HSPC fraction, we further classified this subset using the K nearest-neighbor classification method, resulting in distinct subtypes that were subsequently clustered into HSC/multipotent progenitors (MPP), lymphomyeloid primed progenitors (LMPP), MK and erythroid progenitors (MEP), erythroid progenitors, common lymphoid progenitors (CLP), and granulocyte–monocyte progenitors (GMP)/monoblasts (enriched) subpopulations (Supplementary Fig. S2A). Annotation of each HSPC subpopulation was based on comprehensive transcriptional analysis, including *CD34* expression (highly expressed in HSC/MPPs, LMPPs, CLPs but gradually deceased in GMP/monoblasts and erythroid progenitors; Supplementary Fig. S2B), genes indicative of cell-cycle status (cells in the HSC cluster were predominantly retained in a noncycling (G_1) phase; Supplementary Fig. S2B), gene enrichment scores to identify HSPC subsets (ref. 27; Supplementary Fig. S2C) and expression of genes indicative of HSPC type (*HLF*, *AVP*, and *HES1* for HSCs, myeloid markers *LYZ*, *MPO*, and *S100A8/A9* for GMPs, B cell lineage marker *CD79A* for CLPs and erythroid markers *CA1*, *HBB*, and *HB* for MEPs; Supplementary Fig. S2D and S2E; ref. 26). Trajectory analysis was congruent with the view that HSCs are at the basis of a cellular hierarchy giving rise to erythroid, myeloid, and lymphoid progeny (Supplementary Fig. S2F).

HSC Heterogeneity in the Human Native BM

scRNA-seq studies in mice have revealed transcriptional differences among HSCs, providing an explanation for their functional heterogeneity. Distinct transcriptomes discern long-term (LT), low-output HSCs that self-renew rather than proliferate or differentiate from short-term (ST), high-output HSCs that provide lineage output toward mature progeny during normal steady-state hematopoiesis (28–30). Whether a similar hierarchy of HSCs, reflected in their transcriptome, exists within the HSC pool in human native hematopoiesis has remained largely unknown.

Subclustering of the human HSC/MPP population distinguished 5 subsets (HSC 0–4; Fig. 1C). Cluster 0 constitutes 23.85% ± 1.18% of the HSC pool (Fig. 1C). The transcriptional signature of this cluster 0 had a strong relationship with the transcriptional signature previously reported for low-output LT-HSCs in mice (28, 31), whereas clusters 1–4 displayed strong transcriptional congruence with signatures of high-output ST-HSCs (Fig. 1D).

The "low-output" HSC cluster 0 was also enriched for HSC signatures previously associated with platelet/MK-biased HSCs (28, 31), previously demonstrated to reside at the apex of the hematopoietic stem cell hierarchy (ref. 32; Fig. 1D).

Transcriptional similarity of cells in cluster 0 with murine LT-HSCs included expression of genes associated with self-renewal and quiescence such as *Mllt3*, *Socs2*, *Txnip*, and *Ndn*, MHC class II components [*Cd74, H2-Eb1(HLA-DRB1)*], and transcription regulators (*Hlf*, *Hes1*; Fig. 1E; Supplementary Table S2). Significantly differentially expressed genes in clusters 1–4 included *CDK6*, previously reported to be a critical regulator for the transition of LT-HSCs to ST-HSCs and MPPs (33, 34) and *FLT3* (Fig. 1E).

Gene set enrichment analysis (GSEA) demonstrated transcriptional activation of interferon and STAT activation–related inflammatory signaling (TNF signaling via NFκB;

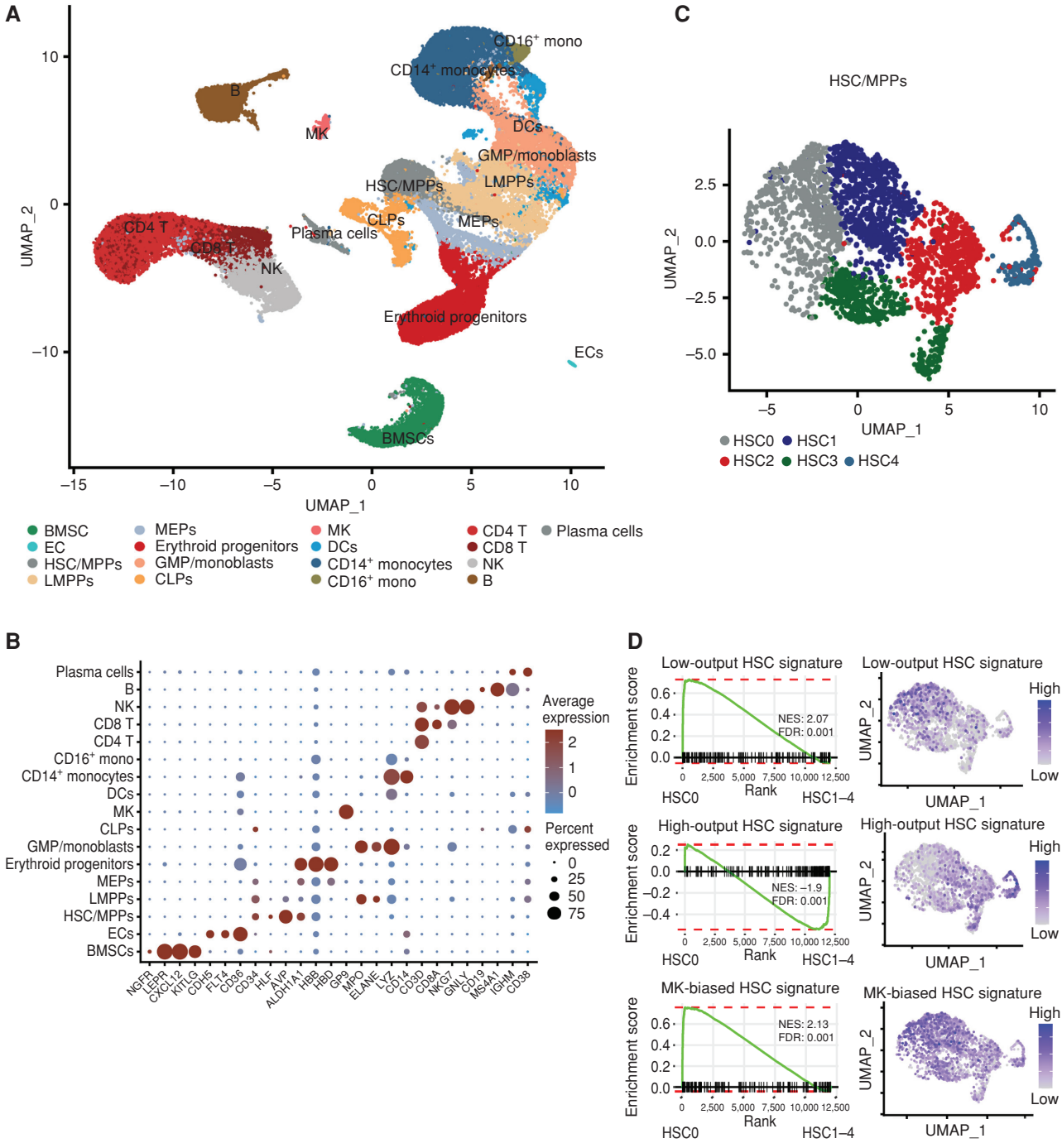

Figure 1. A cellular taxonomy of the human NBM. **A,** Uniform manifold approximation and projection (UMAP) plot of mononuclear cells from BM aspirates, representing 46,740 cells from 4 healthy donors. GMP, granulocyte–monocyte progenitors; MPP, multipotent progenitors; LMPP, lymphomyeloid primed progenitors; CLP, common lymphoid progenitors; MEP, megakaryocytes and erythroid progenitors; EC, endothelial cells. **B,** Expression of cell type–defining genes across all cell types. Color scale and dot size reflect levels and percentages of cells with detectable gene expression. **C,** Heterogeneity of the HSC/MPP population reflected in a UMAP plot, representing 2,763 cells. **D** and **E,** Identification of low-output HSCs (cluster 0) and high-output (clusters 1–4) HSC/MPPs, based on transcriptional homology with these subsets identified in mice. **D,** Gene signatures for low-output, high-output, and megakaryocyte (MK)-biased HSCs in the HSC/MPP subpopulations. (*continued on next page*)

interferon gamma response; IL2–STAT5 signaling) in the HSC-0 cluster (Fig. 1F), reminiscent of an inflammatory transcriptional signature defining a subset of CD74^{high} MHCII^{high} HSCs resistant to myeloablation in mice (35). Interestingly, human cluster-0 HSCs display concomitant overexpression of genes encoding proteins inhibiting inflammation, including *TNFAIP3* (A20; ref. 36) and all members of the NR4A subfamily of nuclear receptors (*NR4A1*, *NR4A2*, and *NR4A3*; Fig. 1E), previously shown to protect LT-HSCs against DNA damage and repress the proliferative inflammatory response

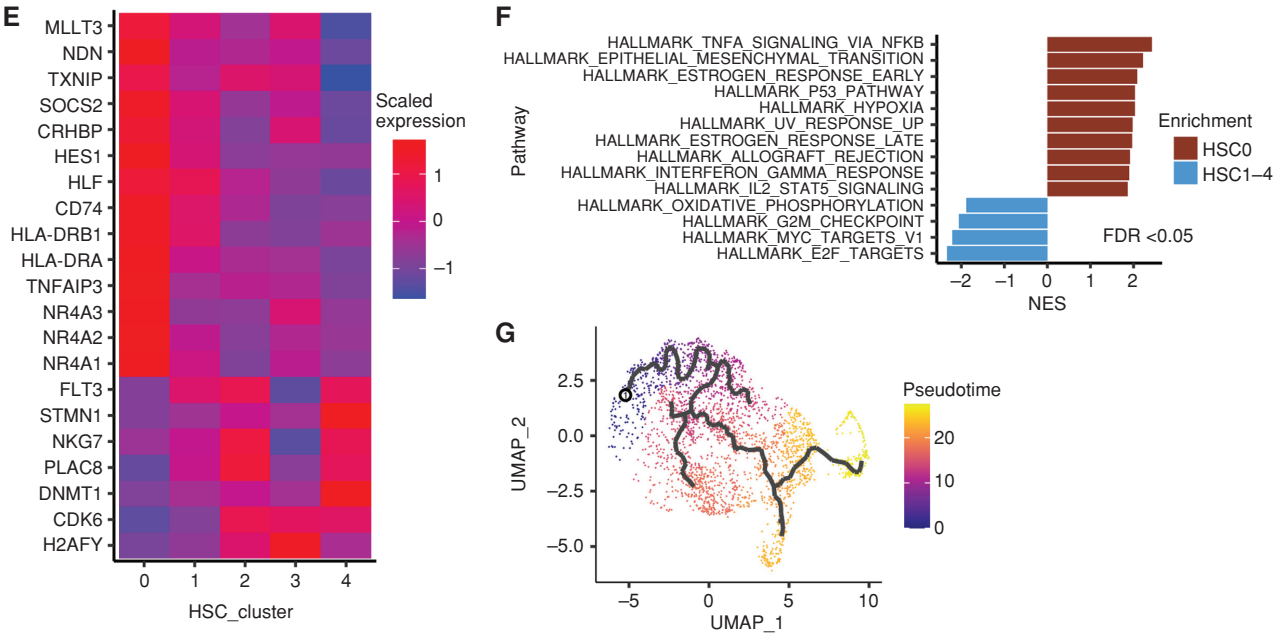

Figure 1. ***(Continued)*** **E,** Heat map showing differential expression of genes between clusters. **F,** Differentially expressed transcriptional programs in HSC cluster 0 in comparison with clusters 1–4, as demonstrated by Hallmark analysis. Positive normalized enrichment score (NES) reflects programs enriched in cluster 0, whereas negative scores indicate enrichment in clusters 1–4. FDR <0.05. **G,** Predicted HSC lineage progression by trajectory analysis. Calculated pseudotime is represented by color scale. HSC cluster 0 is set as a starting point.

of HSCs (37, 38), whereas cell-cycle-related Hallmark gene signatures (E2F targets and G_2–M checkpoint) were significantly enriched in clusters 1–4 (Fig. 1F). Cell trajectory analysis was congruent with the notion that the HSC-0 subset may be at the base of a cellular hierarchy with differentiation trajectories toward HSC clusters 1–4 (Fig. 1G).

Collectively, the data reveal the existence of distinct transcriptional subsets within the HSC/MPP population in human native hematopoiesis, suggesting a linear hierarchy from low-output LT-HSCs to high-output ST-HSC and MPPs, that has previously been demonstrated in mice.

LEPR$^+$ Stromal Cells Are the Main Predicted Source of Cellular Signaling in the Human BM

The generation of a comprehensive cellular taxonomy allows the assessment of predicted cellular interactions in the human BM. We analyzed the predicted intercellular communication between all retrieved cell types based on possible ligand–receptor cross-talk with CellChat, which predicts the major signaling routes and how they integrate into cellular function, using network analysis and pattern recognition approaches (39), revealing a complicated cell interaction network in which all cell types were involved (Fig. 2A).

BMSCs were identified as a key "communication hub" in these analyses, with predicted signaling routes to almost all other cell types in the human marrow, with a predicted magnitude of signaling interaction exceeding that of any other cell population in the marrow (Fig. 2A). This predicted signaling included well-established interactions of BMSCs with HSPCs via KITLG (SCF; to HSC/MPPs, LMPPs, MEPs, and erythroid progenitors; ref. 9) and all immune subsets via CXCL12 (10, 11, 40), lymphoid cells via IL7 (to CLPs, CD4$^+$ T, CD8$^+$ T, and NK; refs. 4, 41) myeloid cells via CSF1 and IL34 (to GMP/monoblasts, DCs, CD14$^+$ monocytes, and CD16$^+$ monocytes; ref. 42), ECs via VEGF and ANGPTL (43), and predicted autocrine signaling via IGF, BMP, TGFβ, and adiponectin, previously implicated in fate-decision signaling (Fig. 2B).

Collectively, the data describe a cellular taxonomy of the stromal and immune environment of the human NBM and their predicted intercellular signaling, unveiling a predicted central role of BMSCs, not only in the homeostatic regulation of HSCs and HSPC subsets but also all innate and adaptive immune cells, in line with experimental data from mouse studies (9, 12).

Stromal Cell Heterogeneity in the Human BM

BMSCs, as shown in mice, represent a heterogeneous population with pleiotropic function in tissue homeostasis and support of distinct hematopoietic cell types (44, 45). Heterogeneity is, in part, related to anatomic localization (endosteal vs. medullary localized BMSCs), but also within the medullary fraction of BMSCs (likely best represented in BM aspirates), heterogeneity exists in mice (2). Whether such heterogeneity exists in humans has remained largely unknown. The robust representation of stromal cells in our datasets allowed for addressing this question.

Subclustering of the BMSC population distinguished 4 subsets (BMSC-0-3; Fig. 2C). All BMSC clusters expressed the sinusoidal stromal HSPC niche marker *LEPR* (9), albeit at different levels, as well as preadipocytic markers (*LPL*, *ADIPOQ*, and *CD36*) and HSC niche factors (*CXCL12*, *KITLG*, and *ANGPT1*; Fig. 2D; Supplementary Fig. S3A), whereas expression of osteolineage differentiation markers (*BGLAP*,

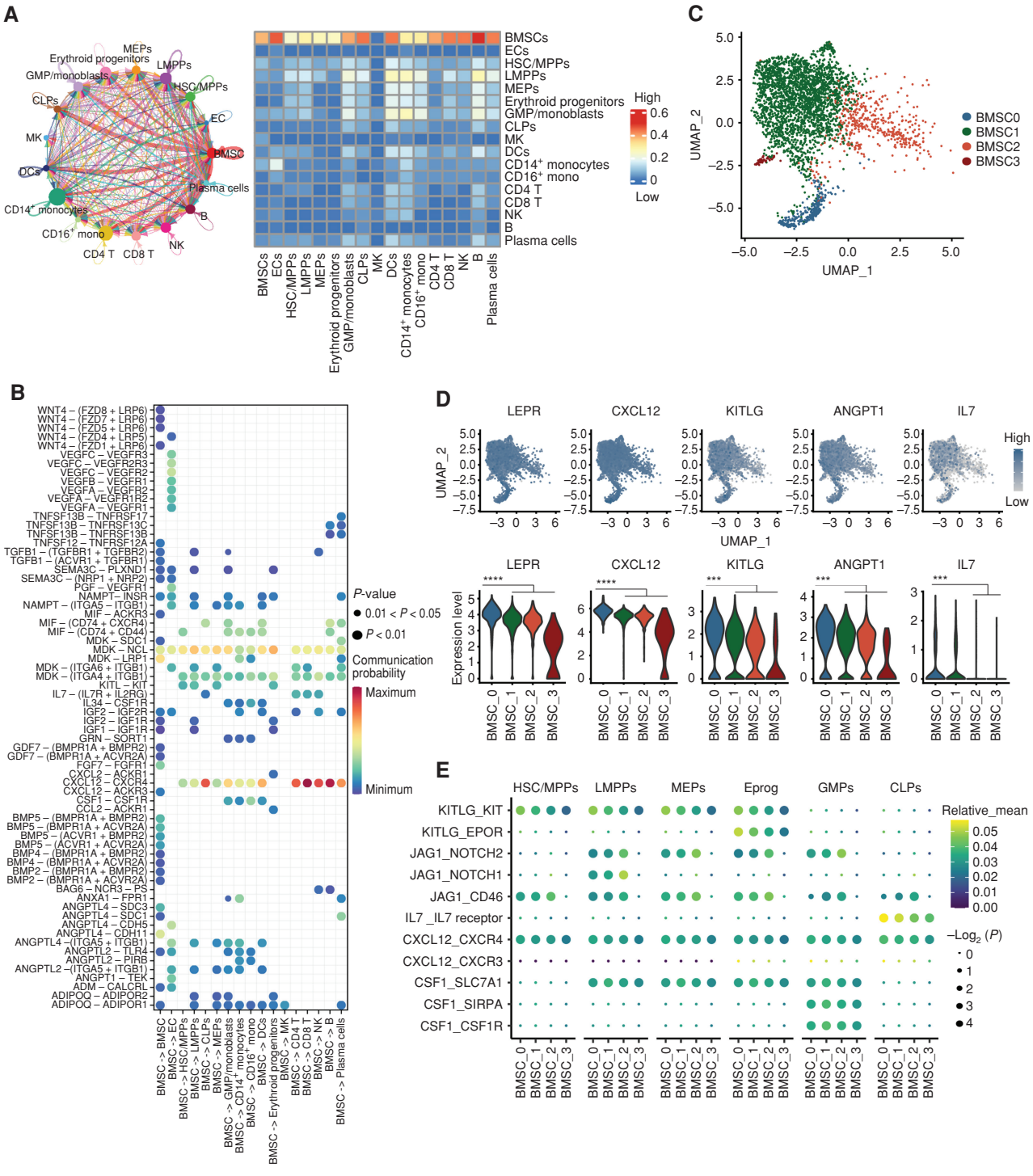

Figure 2. Transcriptional identification of BMSC heterogeneity in the human NBM. **A,** Predicted cellular interactions based on transcriptional networking by CellChat, identifying BMSCs as the dominant source of signaling to all other cells. In the circle plot, colors represent signal senders and width represents signal strength. In the heat map, signal strength is represented by the color scale. **B,** Predicted ligand–receptor interactions between BMSCs and other cell types. Color scale and dot size represent the probability and *P* value of interactions, respectively. **C,** Heterogeneity of the BMSC population reflected in the uniform manifold approximation and projection (UMAP) plot representing 3,236 cells. **D,** Differential expression of *LEPR* and genes encoding key HSPC regulatory factors in BMSC subset 0 represented by UMAP and Violin plots. ***, FDR-adjusted *P* value (P_{adj}) < 0.001. ****, P_{adj} < 0.0001. Differential gene-expression analysis is performed using the pseudoDE R package at the sample level (pair-wise comparison in individual samples). **E,** Relative strength of predicted HSPC-supportive signaling originating from distinct BMSC subsets, as assessed by CellphoneDB. Color scale and dot size represent the relative mean strength and *P* value of interactions, respectively.

RUNX2, and *SPP1*), chondrocyte differentiation markers (*SOX9*, *ACAN*, and *COL2A1*), fibroblast markers (*S100A4* and *SEMA3C*), and pericyte markers (*NES*, *NG2*, and *ACTA2*) could not be detected or were lowly expressed (Supplementary Fig. S3A).

These findings seem consistent with the notion that the BMSCs captured in our analyses represent the human equivalent of the sinusoidal *Lepr*-expressing stromal niche cells in mice that display adipogenic differentiation capacity (24, 46) and are essential for HSPC maintenance (4, 9). Other microenvironmental cells, such as ECs, pericytes, and osteoblasts, could not be retrieved from human BM aspirates or only in numbers too low to perform robust analyses (in the case of ECs).

The BMSC-0 subset, comprising 10.5% ± 5.11% of all stromal cells, displayed the highest expression of *LEPR* and genes encoding critical HSPC regulatory factors (*CXCL12*, *KITLG*, *ANGPT1*, and *IL7*) in comparison with other clusters (Fig. 2D). Transcriptome-wide comparison of this subset with the other stromal subsets revealed differential expression of 443 genes (144 upregulated and 299 downregulated, $P_{adj} < 0.05$; Supplementary Fig. S3B; Supplementary Table S3).

Ligand–receptor analysis revealed that the BMSC-0 subset had the strongest predicted KITLG–KIT, CXCL12–CXCR4, and IL7–IL7 receptor interaction with HSPCs, whereas these interactions were less strong in other clusters (BMSC-1, -2, and -3; Fig. 2E). BMSC-0–derived KITLG was predicted to signal to all HSC subsets (HSC0-4), whereas other interactions, in particular signaling via the CD74 receptor, were predicted to be strongest to the LT-HSC subset of HSCs (Supplementary Fig. S3C).

Taken together, the data indicate that heterogeneity exists within the human BMSC population with a minor subset, characterized by the highest expression of genes encoding critical HSPC maintaining factors, predicted to have the strongest interactions across HSPC subsets, particularly LT-HSCs.

A Cellular Taxonomy of Human *NPM1*-Mutated AML

Earlier approaches to establish cellular hierarchies in human AML have focused on hematopoietic cells (47), precluding the assessment of interactions between rare cell populations such as HSPCs and their stromal niches and their potential involvement in AML pathogenesis. We, thus, generated scRNA-seq tissue maps to establish the cellular taxonomy of the BM in AML with mutations in the gene encoding nucleophosmin (*NPM1*), among the most frequently mutated genes in AML, representing approximately 30% of newly diagnosed patients with AML (48).

BM aspirates from six patients with *NPM1*-mutant (*NPM1m*) AML at diagnosis (median age 53.5; range, 39–59 years; Supplementary Table S1) were sorted and subjected to scRNA-seq, according to the strategy described for NBM, resulting in transcriptomes of 49,758 cells comprising the taxonomy of the BM in *NPM1m* AML (Fig. 3A). The cells representing the clusters annotated within the NBM could largely be retrieved from the AML BM, although disruption of architecture within defined populations was observed, as described below.

Inflammatory Remodeling of LEPR$^+$ BMSCs in NPM1m AML

The predicted central role of LEPR$^+$ BMSCs as intercellular signal traffickers in the human NBM raised the question of whether, and how, LEPR$^+$ BMSC characteristics are disrupted in AML and if alterations could contribute to disease pathogenesis.

Direct comparison of the BMSC transcriptome at the population level (outlined in Fig. 3A) in AML to normal controls showed significant ($P_{adj} < 0.05$) differential expression of 973 genes (541 genes upregulated and 432 genes downregulated; Fig. 3B; Supplementary Table S4). Among the most upregulated genes in AML were genes associated with inflammatory activation, including *NFKBIA, PTGS2, CD44, CXCL2, CXCL8, TGFβ1*, and *ANXA1*, and genes associated with extracellular matrix (ECM) remodeling, including *LOLX2*, *TGFBI*, *COL5A3*, and *COL6A3* (Fig. 3B; Supplementary Fig. S4A and S4B; Supplementary Table S4), with significant downregulation of genes encoding critical HSPC regulatory genes such as *KITLG*, *CXCL12*, and *IL7* and the gene encoding the HSPC niche marker *LEPR* and preadipocyte marker *LPL* (Fig. 3B; Supplementary Fig. S4A and S4B). This was reflected in gene signatures (GSEA Hallmark) consistent with inflammatory signaling (TNFα signaling via NFκB; IL2–STAT signaling; inflammatory response) among the top upregulated transcriptional signatures and downregulation of signatures associated with adipogenesis in AML BMSCs (Fig. 3C; Supplementary Fig. S4C). Disruption of metabolic pathways was suggested by gene signatures indicative of glycolysis in AML BMSCs (Hallmark Hypoxia; Hallmark Glycolysis) versus oxidative phosphorylation and fatty acid metabolism in normal BMSCs (Fig. 3C; Supplementary Table S4). In addition, the GO terms connective tissue development and cartilage development were also significantly increased in the AML BMSCs (Fig. 3D; Supplementary Fig. S4C), indicative of remodeling of the extracellular matrix.

To assess how this disruption of transcriptional programs in the overall BMSC population relates to BMSC heterogeneity in AML, we performed subclustering of the BMSC population (Fig. 3E). This revealed near loss of the cluster predicted to have the strongest interaction with HSPCs (BMSC-0; 3.53% ± 4.84% vs. 11.02% ± 3.39% in AML and NBM, respectively; $P = 0.044$), with a concomitant relative increase of BMSC-2 (46.4% ± 6.81% vs. 7.85% ± 1.24%; $P = 0.009$; Fig. 3E and F; Supplementary Fig. S4D). Levels of genes encoding critical HSPC maintaining factors were significantly reduced in all BMSC subsets in AML, which was most pronounced for *KITLG* and *IL7*, with dramatic impaired expression in BMSC-0 (Fig. 3G).

The BMSC-2 cluster in AML was transcriptionally characterized by the upregulation of genes and transcriptional programs associated with inflammation (Hallmark: Inflammatory Response) and genes and signatures related to ECM remodeling (Fig. 3H and I). This pattern of inflammatory disruption of BMSC architecture and reduced expression of HSPC factors was consistent among all six *NPM1m* AML samples examined (Supplementary Fig. S4A and S4D).

Stromal inflammation was confirmed *in situ* by demonstrating increased CD44 protein expression, which is a marker of

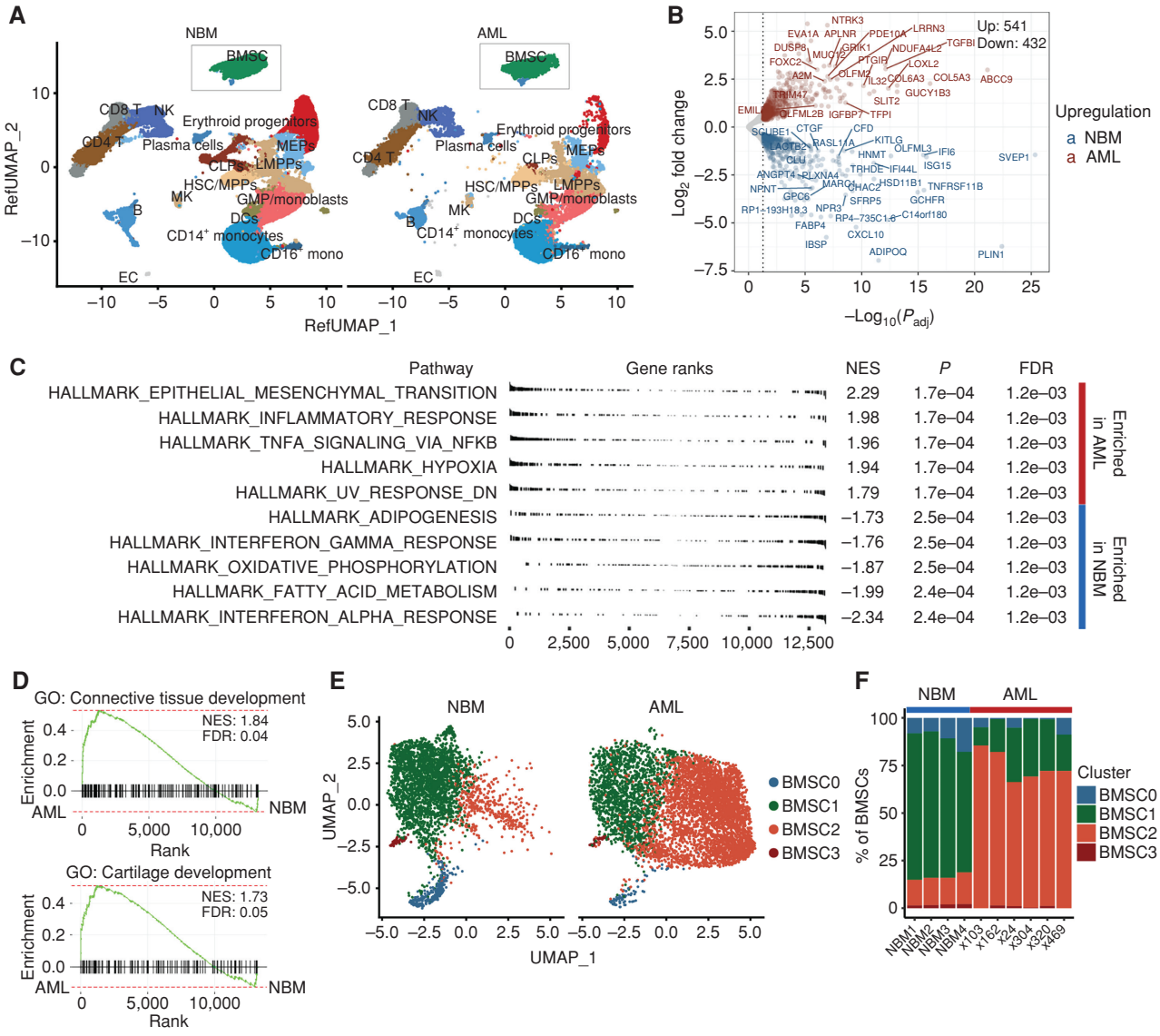

Figure 3. Remodeling of BMSC in *NPM1m* AML. **A,** Uniform manifold approximation and projection (UMAP) distribution of BM cells in NBM and AML. For AML, 49,758 cells from 6 patients are presented. **B,** Volcano plot of differentially ($P_{adj} < 0.05$) expressed genes in BMSCs in AML versus NBM. Differential expression gene analysis is performed at the sample level using the pseudoDE R package. **C** and **D,** Differentially expressed transcriptional programs in BMSCs from AML in comparison with NBM, as demonstrated by Hallmark analysis (**C**) and GO term (**D**). Positive NES (normalized enrichment score) reflects programs enriched in AML, whereas negative scores indicate enrichment in NBM. **E** and **F,** Distribution and frequencies of BMSC subsets in AML and NBM. (*continued on next page*)

stromal activation and inflammation (49), in CD271$^+$(CXCL12$^+$) BMSCs in AML by immunofluorescence on biopsies and flow-cytometric assessment of aspirates (Fig. 3J and K).

Trajectory analysis suggested that the relative reduction of BMSC-0 and increase in the inflammatory BMSC-2 subset may reflect a linear hierarchy characterized by a gradual increase in inflammatory activation accompanied by a loss of expression of HSPC regulatory factors (Supplementary Fig. S4E).

Taken together, the data are congruent with the view that in *NPM1m* AML, BMSCs are remodeled by inflammatory activation, resulting in a dramatic expansion of an inflammatory subset with a concomitant loss of the BMSC subset predicted to support the maintenance of normal HSPCs.

Inflammatory Remodeling of Stromal Niches Is Predicted to Repress High-Output HSCs in AML, Whereas LT-HSCs Are Resistant

Next, we sought to explore the consequences of BMSC remodeling in AML for the residual normal and leukemic hematopoiesis. AML is characterized by suppression of normal hematopoiesis and expansion of clonal cells, but the cellular and molecular mechanisms promoting these processes have remained incompletely understood. Mouse modeling has suggested important contributions of stromal HSPC niches, but the relevance for human AML has remained uncertain.

The localization of *NPM1* mutations at the 3′ terminal coding region of the gene, captured by polyA-RNA-seq, allowed

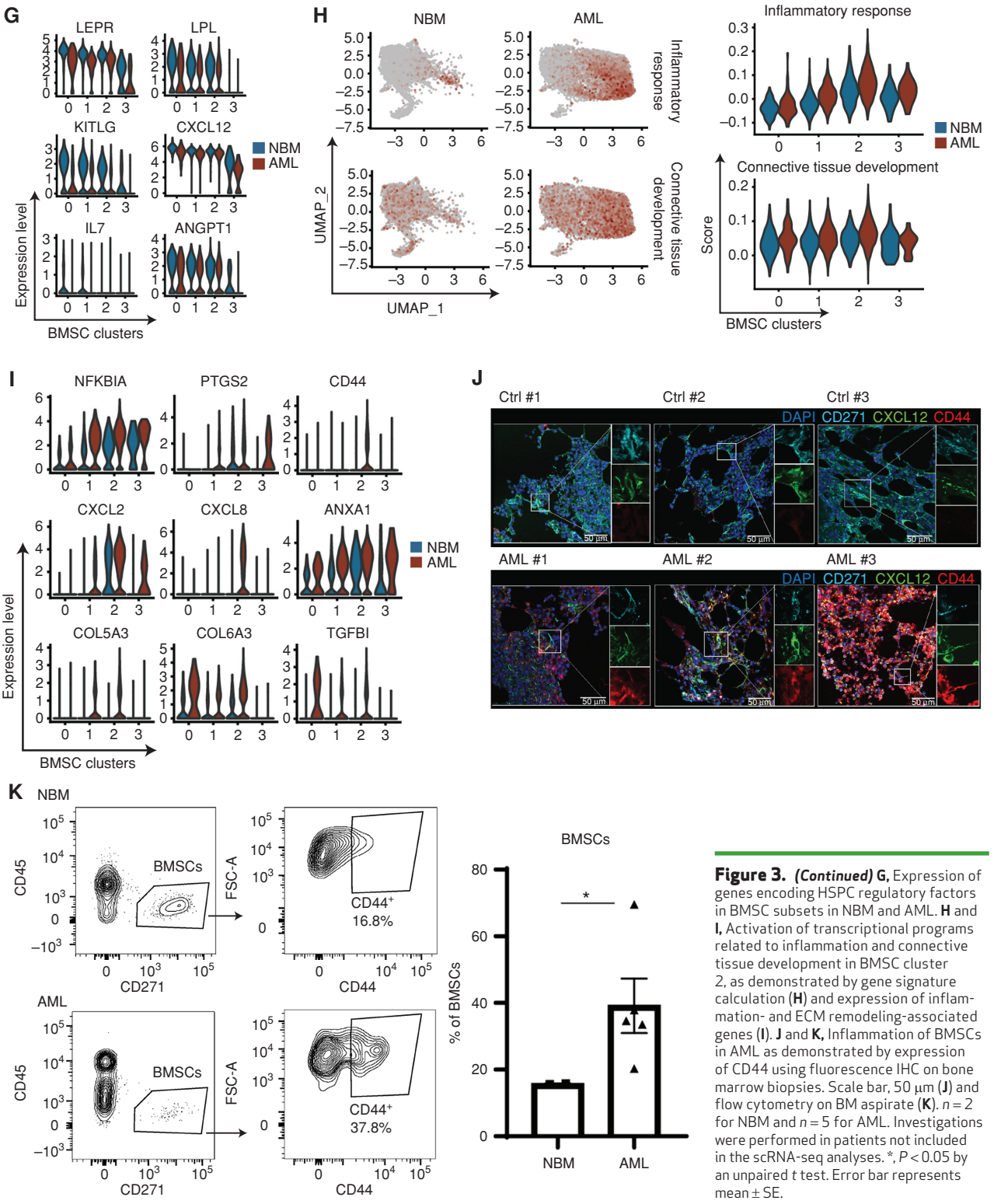

Figure 3. ***(Continued)*** **G,** Expression of genes encoding HSPC regulatory factors in BMSC subsets in NBM and AML. **H** and **I,** Activation of transcriptional programs related to inflammation and connective tissue development in BMSC cluster 2, as demonstrated by gene signature calculation (**H**) and expression of inflammation- and ECM remodeling-associated genes (**I**). **J** and **K,** Inflammation of BMSCs in AML as demonstrated by expression of CD44 using fluorescence IHC on bone marrow biopsies. Scale bar, 50 μm (**J**) and flow cytometry on BM aspirate (**K**). $n = 2$ for NBM and $n = 5$ for AML. Investigations were performed in patients not included in the scRNA-seq analyses. *, $P < 0.05$ by an unpaired t test. Error bar represents mean ± SE.

us to distinguish *NPM1*-mutant AML cells from their nonleukemic hematopoietic counterparts, by assessing the mutational state of *NPM1* in all cells in the dataset (Fig. 4A and Methods). Analysis of mutation status confirmed that adaptive immune subsets ($CD4^+$/$CD8^+$ T cells, plasma cells, and B cells), NK cells, and BMSCs are of nonleukemic origin in AML. The very small fraction of *NPM1m* cells within these fractions differentially and highly expressed myeloid genes (*AZU1*, *LYZ*, *MPO*, and *ELANE;* Supplementary Fig. S4F), indicative of blast contamination. *NPM1m* leukemic cells reside predominantly within the LMPP and GMP subsets of the HSPC fraction (Fig. 4A and B).

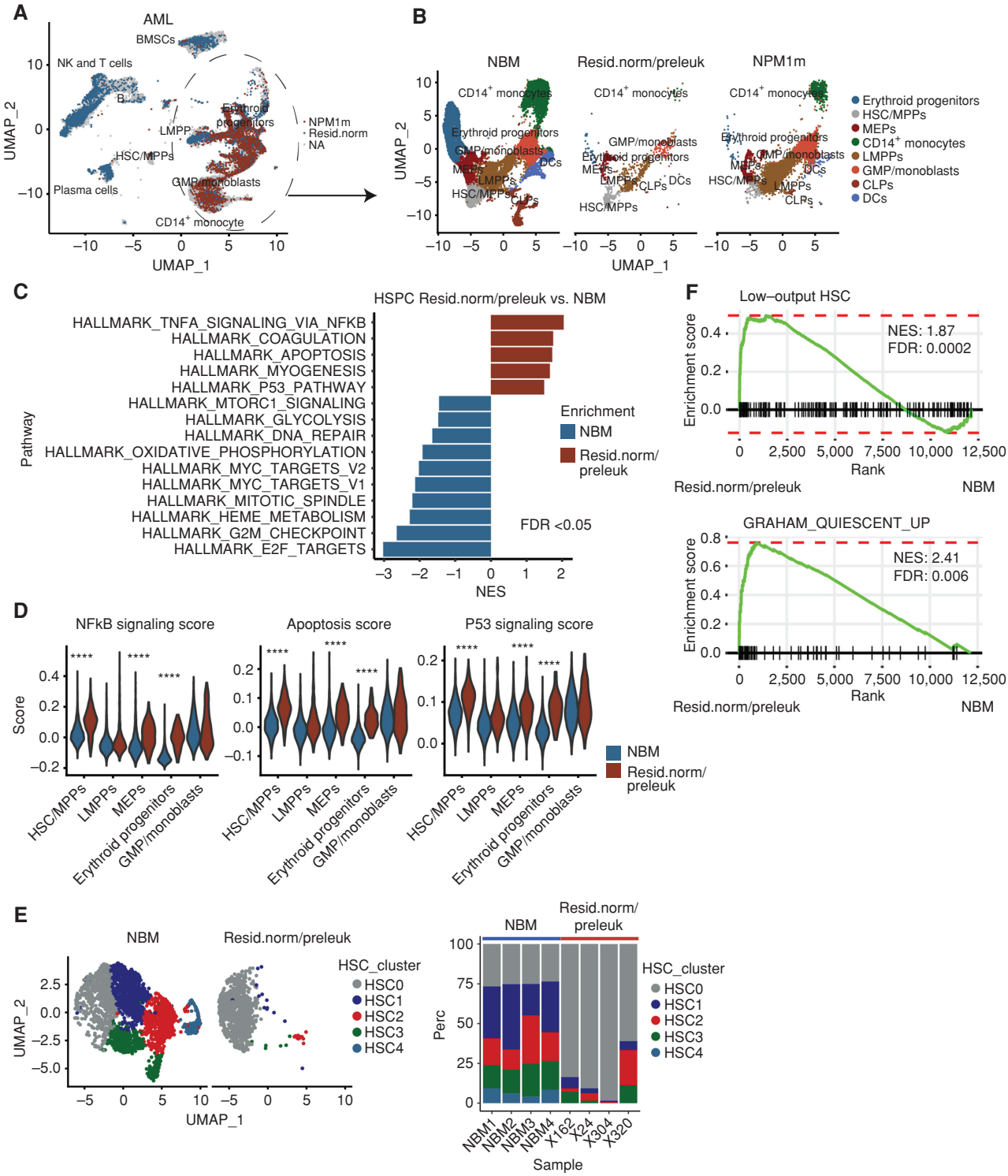

Figure 4. Nonleukemic hematopoiesis is suppressed in patients with AML, whereas NPM1-mutant cells display relative resistance. **A,** Uniform manifold approximation and projection (UMAP) distribution of *NPM1*-mutant (*NPM1m*; red) and residual normal/preleukemic cells (resid.norm/preleuk; blue) in the AML BM. NA (gray), not assignable. **B,** Distribution of normal, residual normal/preleukemic, and *NPM1m* cells within the HSPC and myeloid fractions in NBM and AML. **C,** Differentially expressed transcriptional programs in residual normal/preleukemic HSPCs in AML compared with HSPCs in NBM, as demonstrated by Hallmark analysis. Positive NES (normalized enrichment score) reflects programs enriched in residual normal, whereas negative scores indicate enrichment in NBM. All cells in HSC/MPPs, LMPPs, MEPs, erythroid progenitors, and GMP/monoblasts clusters were analyzed. **D,** Overexpression of Hallmark transcriptional signatures indicative of NFkB signaling, Apoptosis and P53 signaling in residual normal/preleukemic HSPC in comparison with their counterparts in the human NBM. ****, $P_{adj} < 0.0001$ by the Wilcoxon test. **E,** Distribution and frequencies of HSC/MPP subsets of residual normal/preleukemic HSPCs in comparison with NBM. In two (out of six) AML samples, insufficient cells could be retrieved in the HSC/MPP subset for analysis. **F,** Enrichment of transcriptional programs indicative of low-output, quiescent, HSCs in residual normal/preleukemic HSC/MPPs in AML in comparison with their counterparts in the human NBM. (*continued on next page*)

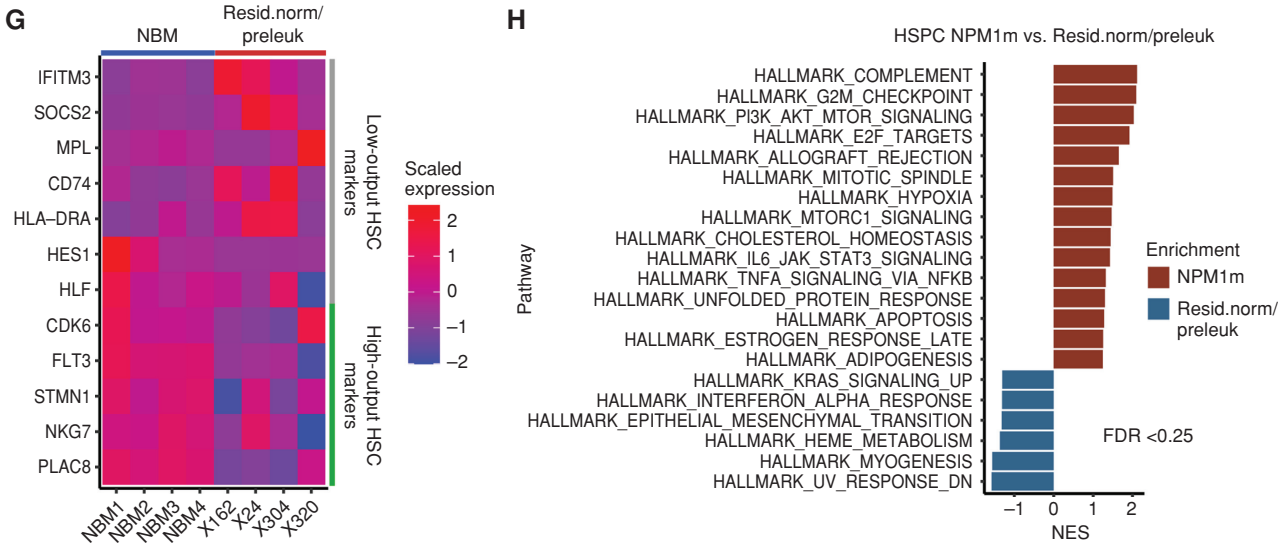

Figure 4. ***(Continued)*** **G,** Heat map for low- and high-output HSC marker genes in NBM and residual normal/preleukemic HSC/MPP population across all samples. **H,** Differentially expressed transcriptional programs in *NPMm* cells within the HSPC subsets in comparison with residual normal/preleukemic HSPCs, as demonstrated by Hallmark analysis. Positive NES (normalized enrichment score) reflects programs enriched in *NPM1m* HSPCs, whereas negative scores indicate enrichment in residual normal/preleukemic HSPCs. All cells in HSC/MPPs, LMPPs, MEPs, erythroid progenitors, and GMP/monoblasts clusters were used in the analysis.

The remodeling of stromal niches in human AML, in particular the loss of stromal subsets predicted to have the strongest supportive interaction with HSPCs, and the marked downregulation of KITLG-encoding *SCF*, are predicted to have major consequences for residual normal hematopoiesis. Depletion of Scf from *Lepr*$^{+}$ BMSCs in mice results in cytopenia, hypocellularity of the marrow, and a reduction in HSC number (5), indicating that stromal SCF is critical for the maintenance of normal HSCs and hematopoiesis. *Lepr*$^{+}$ BMSC-derived Scf is also critical for the maintenance of kit^{+}-restricted hematopoietic progenitors (in particular CLPs and MEPs and to a lesser extent CMP and GMP; ref. 9).

Ligand–receptor analyses confirmed that BMSC–HSPC interactions deemed critical for HSPC maintenance, survival, and proliferation (such as KITLG–KIT and CXCL12–CXCR4) were attenuated in nonleukemic HSPC subsets in AML in comparison with their counterparts in NBM (Supplementary Fig. S5A). It is relevant to note that these nonleukemic HSPCs in the AML marrow comprise both healthy, unmutated, HSPCs and "preleukemic" HSPCs carrying founder mutations in genes such as *DNMT3A* and *TET2* (Supplementary Table S1), which cannot be reliably detected by 10× scRNA-seq. We thus evaluated the cellular changes in the residual normal/preleukemic HSPC compartment associated with the predicted disruption of niche signaling. The HSPC fraction in AML displayed a relative reduction of erythroid progenitors (17.41% ± 9.77% vs. 6.31% ± 5.74% of the HSPC fraction in NBM and AML, respectively, $P = 0.1$) and GMP/monoblasts (22.08% ± 3.29% vs. 12.14% ± 7.15%, $P = 0.02$), as well as near loss of the CLP population (8.85% ± 3.79% vs. 0.15% ± 0.378%, $P = 0.019$; Fig. 4B), recapitulating observations in mice with depletion of Scf from *Lepr*$^{+}$ BMSCs (9).

In line with the notion that residual normal HSPCs in AML may be affected by the loss of stromal niche factors, and in particular, SCF propagating survival and proliferation signals, which occur via activation of PI3K–AKT–MTORC signaling (50, 51), GSEA and Hallmark pathway analyses demonstrated enrichment of inflammatory and apoptotic signatures in residual normal/preleukemic subsets in comparison with their counterparts in the human NBM (Hallmark: TNFα via NFκB; Hallmark: apoptosis and Hallmark: P53 pathway) with concomitant depression of signatures indicative of MTORC signaling, active cellular metabolism, and proliferation (Hallmark: TORC1 signaling; Hallmark: E2F targets; Hallmark: G_2–M checkpoint, Hallmark: Mitotic spindle and Hallmark: Oxidative phosphorylation; Fig. 4C and D). Interestingly, these transcriptional programs indicative of cellular stress were activated most extensively in residual normal/preleukemic cells within the HSC/MPP, MEP, and erythroid progenitor populations (Fig. 4D), the progenitor cells known to be most repressed in AML (resulting in anemia and thrombocytopenia).

The CD34^{high} HSC compartment was largely of nonleukemic origin (with only 3.66% ± 2.88% of cells within this HSC/MPP population detected positive for *NPM1* mutation; Fig. 4A), in line with the existing notion that *NPM1m* AML has low expression of CD34 and may find its origin in transformation of committed progenitors (52). Reclustering of the HSC population showed that, strikingly, the ST, high-output, HSC/MPP subsets (HSC-1–4) were almost completely depleted from the residual normal/preleukemic HSC pool in AML (74.78% ± 1.29% vs. 16.47% ± 16.12% in NBM and AML, respectively, $P = 0.005$) with relative conservation of the LT, low-output, HSC-0 subset (Fig. 4E). In line with this observation, the gene signatures indicative of low-output HSCs and quiescence were significantly enriched in the residual normal/preleukemic HSCs (Fig. 4F), whereas the high-output HSC marker genes such as *FLT3*, *STMN1*, *PLAC8*, and *MPO*

were downregulated (Fig. 4G; Supplementary Table S5). The remodeling of the HSC compartment was also found in a patient (X320) in which no founder mutations were detected (Supplementary Table S1), suggesting that the relative loss of "high-output" HSCs is not caused (solely) by the presence of founder mutations such as *DNMT3A* and *TET2* in these cells.

The finding that this specific HSC subset, predicted to be the LT-repopulating subset of HSCs resistant to chemotherapy in mice, resists inflammatory stress seems consistent with the long-standing observation that the human BM can reconstitute normal hematopoiesis after chemotherapeutic eradication of leukemic cells.

Importantly, *NPM1m* cells within the HSPC fraction, predominantly found within the LMPP and GMP subsets (Fig. 4B), showed preservation of transcriptional MTORC1 and survival signaling (Fig. 4H), suggesting relative resistance to the factors driving the cellular stress in comparison with residual normal HSPCs. Moreover, several interactions were predicted between inflammatory molecules encoded by genes differentially expressed in the "inflamed" BMSC subset (BMSC-2) and the LMPP-like, GMP-like and/or monocyte-like *NPM1m* AML cells, including HGF–CD44, IL6–IL6 receptor, and JAG1–NOTCH1/NOTCH2 interactions (Supplementary Fig. S5A), which have been reported to drive the initiation, proliferation, and/or chemoresistance of AML (17, 53, 54).

Collectively, the scRNA-seq data, in conjunction with previously established relevance of niche factors for normal hematopoiesis in mice, support the view that niche remodeling by inflammatory activation and suppression of HSPC maintenance factors in AML suppress normal hematopoiesis, whereas LT-HSCs and *NPM1m* leukemic cells are relatively resistant to the deprivation of supportive signaling from stromal niches. In addition, inflamed BMSCs express factors previously associated with leukemia propagation. Niche remodeling is thus predicted to be a driving force in the competitive advantage of mutated cells over their normal and preleukemic counterparts in leukemogenesis.

Additionally, LEPR$^+$ BMSC transcriptional remodeling in AML is predicted to affect cellular signaling to lymphoid immune subsets (CD4 T, CD8 T, NK, B, and plasma cells) in the leukemic bone marrow (Supplementary Fig. S5B). This complex cellular taxonomy of the intercellular signaling defining human AML is anticipated to provide a resource to instruct future experimental interrogation of the relevance of these interactions.

TNFα from Activated Immune Cells May Drive Inflammation and Loss of *KITLG* Expression from BMSC Niches in AML and Represses Normal Hematopoiesis

The scRNA-seq analyses suggested that the disruption of BMSC architecture in AML may reflect inflammatory activation of LEPR$^+$ BMSCs. To provide experimental support for this view, we tested whether secreted inflammatory factors could induce the inflammatory alterations observed in the BMSC compartment in AML. The significantly enriched gene signature "TNFα signaling via NFκB" (Fig 3C) suggested that TNFα may be one such factor. TNFα levels have earlier been demonstrated to be increased in the plasma of patients with AML (55) and *TNF* is overexpressed in AML at the transcriptional level (Supplementary Fig. S6A). The scRNA-seq data showed that *TNF* is highly expressed in adaptive and innate immune cells (CD8 T cells and NK cells) and myeloid lineage cells (GMP/monoblasts and CD14$^+$ monocyte populations) in *NPM1m* AML (Supplementary Fig. S6B and S6C), whereas its canonical receptor *TNFRSF1A* is predominantly expressed in LEPR$^+$ BMSCs (Supplementary Fig. S6D), predicting that LEPR$^+$ BMSCs could be one of the cell types in AML most affected by TNFα signaling.

To test whether TNFα can induce inflammatory remodeling of LEPR$^+$ BMSCs and attenuate normal hematopoiesis, we performed an *in vivo* experiment, injecting C57BL/6 mice intraperitoneally with recombinant TNFα (Fig. 5A). This resulted in cytopenia (anemia and thrombocytopenia; Fig. 5B) and a significant reduction of the frequency of LEPR$^+$ stromal cells within the nonendothelial (CD45$^-$Ter119$^-$CD31$^-$CD144$^-$CD51$^+$Sca1$^-$) niche (Fig. 5C and D). RNA-seq confirmed high levels of *Kitlg* and *Cxcl12* expression, specifically in the LEPR$^+$ stromal cell population, in line with the notion that these cells represent HSPC niches (Fig. 5E; ref. 5). TNFα exposure induced overexpression of inflammatory markers, including *Cd44* and *Cxcl2*, with concomitant downregulation of *Kitlg* and *Cxcl12* (Fig. 5E), in line with the notion that TNFα leads to stromal inflammatory remodeling with subsequent reduction of HSPC niche cells, recapitulating findings in human AML. This was further associated with a reduction in BM cellularity and depletion of distinct subsets of HSPCs, in particular MPPs (Lin$^-$cKIT$^+$Sca1$^+$CD48$^-$CD150$^-$), CMPs (Lin$^-$cKIT$^+$Sca1$^-$CD34$^+$CD16$^-$), GMPs (Lin$^-$cKIT$^+$Sca1$^-$CD34$^+$CD16$^+$), and MEPs (Lin$^-$cKIT$^+$Sca1$^-$CD34$^-$CD16$^-$; Fig. 5F), resembling the reduction in MPPs and committed progenitor fractions in human *NPM1m* AML.

To begin testing the functional significance of inflammatory BMSC niche remodeling on normal versus leukemic hematopoiesis using an *ex vivo* coculture system, we exposed human HS-5 stromal cells to TNFα (10 ng/mL) for 24 hours to trigger the inflammatory response, followed by coculturing with either human CD34$^+$ HSPCs or primary *NPM1m* AML cells for 72 hours (Supplementary Fig. S6E). This resulted in a significant reduction of immunophenotypic HSPCs (CD45$^+$Lin$^-$CD34$^+$) and CFU-GEMM (Supplementary Fig. S6E), whereas the number of *NPM1m* AML cells was not affected by the inflammatory activation of stromal cells induced by TNFα (Supplementary Fig. S6E). In line with these *in vitro* findings, *in vivo* administration of TNFα in a well-established MLL-AF9 mouse transplantation model of AML did not result in a reduction of leukemic cells (Supplementary Fig. S6F), while it resulted in a marked decrease in the frequency of LEPR$^+$ BMSCs (Supplementary Fig. S6G). The reduction in the frequency of stromal niches in the MLL-TNFα condition was associated with worsening of anemia and a (nonsignificant) reduction in the number of residual normal MPPs (Supplementary Fig. S6H), recapitulating aspects of the negative effect of TNFα on normal hematopoiesis (Fig. 5).

Together, the data fit a model in which overexpression of TNFα, perhaps in part by activation of the innate and adaptive immune system in *NPM1m* AML, results in suppression of hematopoiesis with relative resistance of clonal leukemic cells. This is associated with inflammatory remodeling of stromal

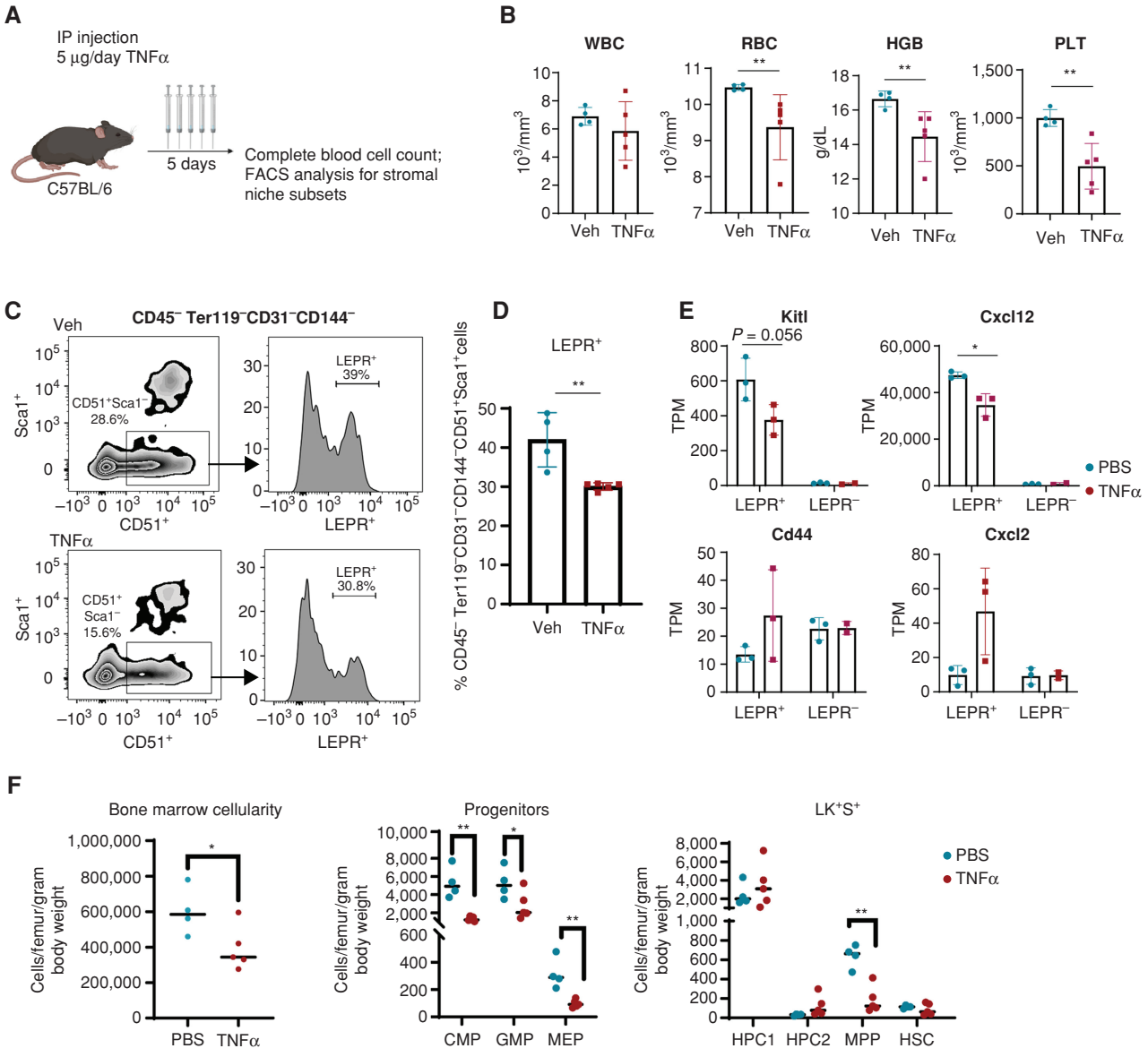

Figure 5. TNFα induces inflammatory remodeling of stromal niches and a reduction in HSPC numbers in mice. **A,** Experimental design of TNFα administration to C57BL/6 mice. Five daily i.p. injections at a dose of 5 μg were administrated followed by flow-cytometric assessment of BM stromal niches in collagenased bone fractions. **B,** Cytopenia (anemia and thrombocytopenia) in TNFα-treated mice. **, $P < 0.01$ by an unpaired *t* test. **C** and **D,** Relative loss of LEPR⁺ BMSCs within the niche fraction upon TNFα exposure. **, $P < 0.01$ by an unpaired *t* test. **E,** Expression of inflammatory makers and HSPC niche factors in CD51⁺ LEPR⁺ and CD51⁺LEPR⁻ BMSCs after TNFα injection in mice. *, $P < 0.05$ by an unpaired *t* test. **F,** Number of total BM cells, committed progenitors, and LKS HSPC subtypes in mice after TNFα injection. *, $P < 0.05$; **, $P < 0.01$ by an unpaired *t* test. Error bar represents mean ± SE. Veh, vehicle; WBC, white blood cell count; RBC, red blood cell count; HGB, hemoglobin; PLT, platelet.

niches predicted to affect the survival and proliferation of HSPC subsets, although direct effects of TNFα on HSPCs have also been demonstrated (56) and cannot be excluded.

Inflammatory Stromal Activation and Impaired Expression of HSPC Factors Is Common Across AML and Is Variable Between Genetic Subtypes and Risk Groups

We next asked the question of whether the inflammatory remodeling of BMSCs in AML was restricted to *NPM1m* cases, or rather a biological commonality in AML across different, distinct, genetic subtypes. To answer this question, bulk RNA-seq was conducted on highly purified CD45⁻CD71⁻CD235a⁻CD31⁻CD271⁺ BMSCs isolated from a cohort of 62 newly diagnosed patients with AML (Supplementary Fig. S7A), uniformly treated within an intensive chemotherapy clinical trial (57) and selected to represent the mutational landscape of AML (Supplementary Table S1). The purity of the sorted stromal population was confirmed by excluding the expression of hematopoietic transcripts (including CD45 (*PTPRC*), *CD34*, *MPO*, and *GYPA*; Supplementary Fig. S7B) and expression of canonical stromal markers (CD271 (*NGFR*), *COL1A1*, CD90 (*THY1*), and *PRRX1* (Supplementary Fig. S7B).

Overall, 1,579 genes were differentially expressed in the AML BMSCs in comparison with age-matched normal controls (n = 8; Supplementary Table S6), including 1,413 upregulated and 166 downregulated genes (Supplementary Table S6). GSEAs revealed differentially expressed gene sets, very similar to those identified by scRNA-seq in the *NPM1m* subset, including enrichment of the signatures indicative of inflammatory activation (TNFα signaling via NFκB; inflammatory response) and hypoxia, as well as depletion of gene sets indicative of adipogenesis and oxidative phosphorylation; Fig. 6A). Consistent with this, expression of the NFκB-related inflammatory genes/cytokines such as *NFKBIA*, *CD44*, *CXCL2, CXCL3*, *CXCL8*, *CCL2*, *LIF*, and *PTGS2* was significantly upregulated in AML and adipogenesis markers (*LPL*, *ADIPOQ* and *CD36)* significantly downregulated (Fig. 6B; Supplementary Table S6). Similarly, the expression of *LEPR* and genes encoding the HSPC regulatory factors CXCL12, KITLG, and ANGPT1 was significantly reduced in AML BMSCs (Fig. 6B), in line with the scRNA-seq data from *NPM1m* patients. Notably, inflammatory activation of BMSC in AML (as represented by the TNFα via NFκB score) was strongly associated with the reduction in expression of HSPC niche genes such as *LEPR*, *CXCL12, KITLG*, and *ANGPT1* (Supplementary Fig. S7C), congruent with the notion that inflammatory activation results in reduction of HSPC niches and downregulation of HSPC factors, as established in our *in vivo* experiments (Fig. 5C–E).

To obtain insight into the heterogeneity of these signatures among genetic subtypes, scores were allocated to individual samples and categorized among genetic subtypes using gene set variation analysis (GSVA; ref. 58; Fig. 6C), revealing that inflammatory scores were relatively high in the *NPM1m* patients and tended to be lower in patients carrying either a *RUNX1*, *ASXL1*, or *TP53* mutation, although heterogeneity existed within these genetic subsets (Fig. 6C). Correlation of BMSC signatures to genetic risk categories as defined by the ELN (ref. 59; shown to be of prognostic relevance in our cohort of 62 patients, as expected; Supplementary Fig. S7D), revealed that patients in the favorable risk category displayed the most pronounced NFκB inflammatory activation and suppression of niche supportive factors (*LEPR*, *KITLG*, and *ANGPT1*; Fig. 6D), whereas BMSCs in the adverse risk group tended to be less perturbed in comparison with NBM.

Together, the data demonstrate that the remodeling of BMSCs, revealed by scRNA-seq in *NPM1m* patients and defined by activation of inflammatory signaling and reduced expression of HSPC maintenance factors associated with the loss of the HSPC niche subset, is a biological commonality in AML and that the extent of this remodeling may vary within and between genetically defined subsets of patients.

Stromal Inflammatory Niche Remodeling and Associated Gene Signatures Are Associated with Favorable Outcome in AML

We next asked the question whether inflammatory remodeling of stromal niches is related to clinical outcomes in AML. The loss of stromal HSPC niche cells has recently been associated with better outcomes upon chemotherapeutic treatment in AML in a mouse model (16). In the MLL-AF9 AML model, genetic depletion of stromal niche cells resulted in delayed relapse after cytarabine treatment (16). The finding that the HSPC niche (BMSC-0) subset of stromal cells is depleted in AML (to varying degrees) as a result of inflammatory remodeling prompted us to interrogate the prognostic value of a transcriptional signature reflecting BMSC remodeling in the context of intensive chemotherapy in human AML.

In order to analyze the correlation between BMSC heterogeneity with clinical outcome in AML, we made a "by-proxy" assessment of BMSC heterogeneity from bulk transcriptomes of all 62 patients using CIBERSORTx, a machine learning method to impute gene-expression profiles and provide an estimation of the relative abundance of cellular subsets in a mixed population (60). The BMSC scRNA-seq dataset was used as a reference, and the relative abundance of all four BMSC subsets was computationally retrieved (Fig. 7A).

In line with our scRNA-seq observations in *NPM1m* patients, the predicted size of the BMSC-0 subset was significantly reduced in this larger AML population, with a concomitant increase in the size of the inflamed cluster (BMSC-2; Fig. 7A). Interestingly, stratifying patients with AML into a "BMSC-0 preserved" group and a "BMSC-0 depleted" group based on the median level revealed that depletion of the BMSC-0 niche subset was significantly associated with better overall survival (5-year OS 57.2% vs. 31.0% of patients; P = 0.041) and reduced risk of relapse (32.0% vs. 65.2% of patients; P = 0.032; Fig. 7B).

Next, we sought to refine this analysis and get better insight into the genes in the remodeled stromal cells that shape this association between niche remodeling and clinical outcomes in AML. To this end, we generated a list of genes significantly differentially expressed in BMSCs in human AML (in comparison with BMSCs in NBM) that intersected with inflammation-associated genes (differentially expressed in AML BMSC cluster 2 vs. other clusters in AML) and HSPC niche genes (differentially expressed genes in NBM BMSC cluster 0 vs. other clusters in NBM), resulting in a list of 189 genes (Fig. 7C; Supplementary Table S7).

By constructing a penalized multivariable Cox regression model through nested cross-validation (61), 13 of 189 genes were identified to be correlated to OS (Fig. 7C and D). The strongest negative association (coefficient: 0.34; overexpressed in the HSPC niche population and related to poor prognosis) was found for *KITLG* (Fig. 7D), indicative of a positive correlation between the loss of the HSPC niche population and favorable outcome. Other genes overexpressed in the HSPC niche population (BMSC-0) or inflammatory population (BMSC-2) and associated with poor OS include *ARPC5L*, encoding an actin-related protein involved in cell migration, *MEDAG*, a positive regulator for adipocyte differentiation, and *PTGDS*, encoding a glutathione-independent prostaglandin D synthase that catalyzes the conversion of prostaglandin H2 (PGH2) to prostaglandin D2 (PGD2; Fig. 7D). Upregulation of the inflamed cluster (BMSC-2) genes *ZBTB21, SPAG9*, *ELL2*, and *SMAD7* (a TGFβ inhibitor positively regulated by inflammatory cytokines; refs. 62, 63), on the other hand, were strongly associated with a favorable outcome (Fig. 7D).

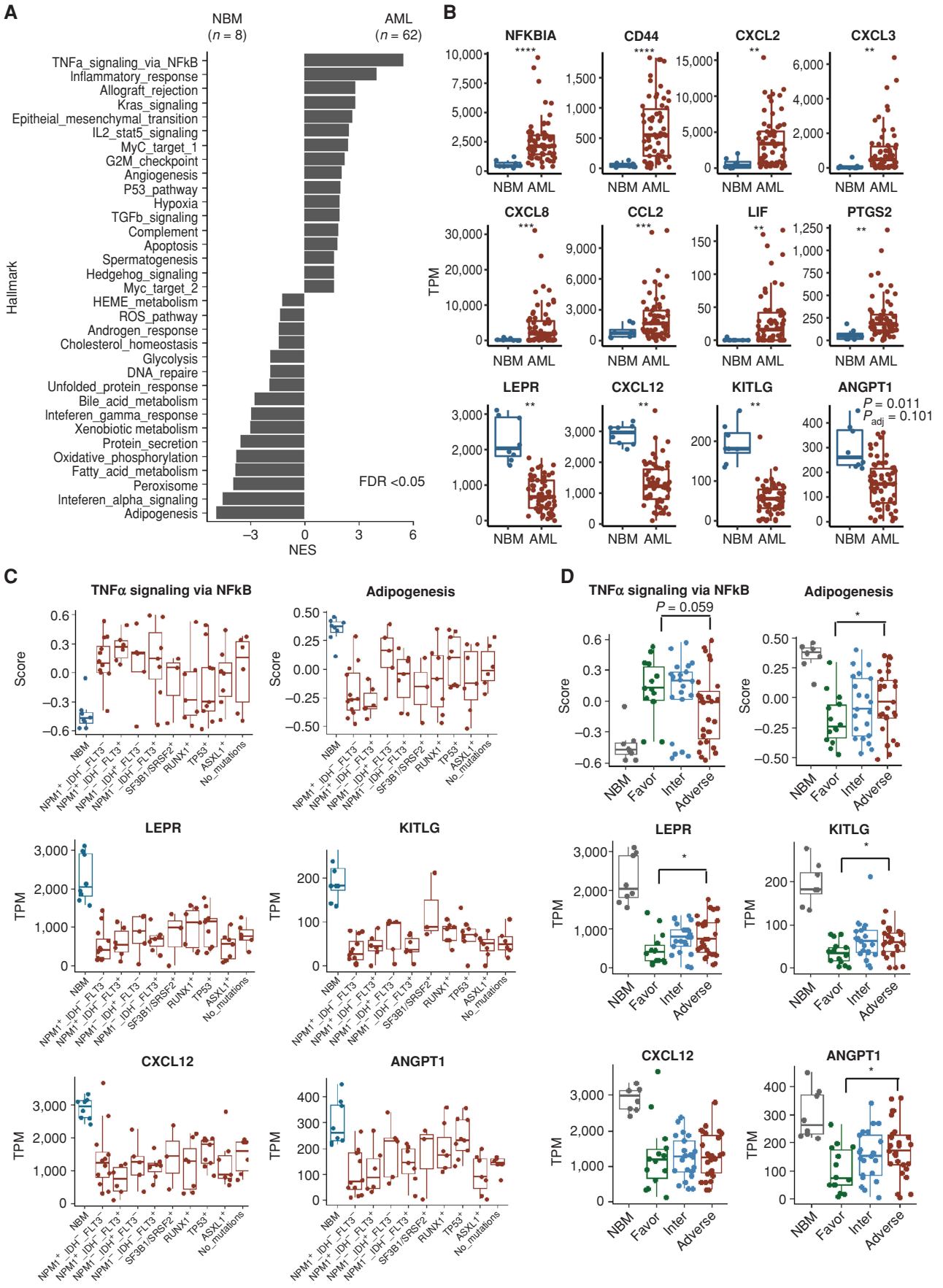
A
NBM (n = 8)
AML (n = 62)
Hallmark
TNFa_signaling_via_NFkB
Inflammatory_response
Allograft_rejection
Kras_signaling
Epitheial_mesenchymal_transition
IL2_stat5_signaling
MyC_target_1
G2M_checkpoint
Angiogenesis
P53_pathway
Hypoxia
TGFb_signaling
Complement
Apoptosis
Spermatogenesis
Hedgehog_signaling
Myc_target_2
HEME_metabolism
ROS_pathway
Androgen_response
Cholesterol_homeostasis
Glycolysis
DNA_repaire
Unfolded_protein_response
Bile_acid_metabolism
Inteferen_gamma_response
Xenobiotic metabolism
Protein_secretion
Oxidative_phosphorylation
Fatty_acid_metabolism
Peroxisome
Inteferen_alpha_signaling
Adipogenesis
FDR <0.05
NES
B
NFKBIA
CD44
CXCL2
CXCL3
CXCL8
CCL2
LIF
PTGS2
LEPR
CXCL12
KITLG
ANGPT1
P = 0.011
P_adj = 0.101
TPM
NBM AML
C
TNFα signaling via NFkB
Adipogenesis
LEPR
KITLG
CXCL12
ANGPT1
Score
TPM
NBM
NPM1+ IDH− FLT3−
NPM1+ IDH− FLT3+
NPM1− IDH+ FLT3−
NPM1− IDH+ FLT3+
NPM1− IDH− FLT3+
SF3B1/SRSF2+
RUNX1+
TP53+
ASXL1+
No_mutations
D
TNFα signaling via NFkB
P = 0.059
Adipogenesis
LEPR
KITLG
CXCL12
ANGPT1
Score
TPM
NBM
Favor
Inter
Adverse

Based on this 13-gene signature, a score was calculated that allowed for stratifying patients with AML into a "BMSC-inflammatory remodeling" group (score^{low}) and a "BMSC niche-preserved" group (score^{high}) based on the median level (Fig. 7D). The low score, "BMSC-inflammatory remodeling" group had significantly better OS (5-year OS 80% vs. 8.6%; $P < 0.0001$) and lower relapse probability (5-year relapse probability 13% vs. 78.4%; $P < 0.0001$; Fig. 7E). Importantly, this significant survival benefit was found throughout all distinct ELN2017 genetic risk categories (Supplementary Fig. S8A).

Finally, we sought to confirm our finding that stromal niche factors, associated with inflammatory remodeling, are associated with outcomes in an independent cohort of patients with AML. Although many of the factors in the prognostic stromal niche gene signature were either not specifically expressed in stromal cells or not detected in published transcriptional datasets of AML, we found the gene *KITLG* (i) to be an important determinant of the prognostic value of the stromal prognostic gene signature (Fig. 7D and F), (ii) to be specifically expressed in BMSCs in the AML taxonomy (Supplementary Fig. S8B), and (iii) to be detectable in publicly available transcriptional datasets generated from BM aspirates of patients with AML (18–65 years, treated with intensive chemotherapy), namely, the TCGA-LAML (64) and Bohlander (GSE37642; ref. 65) cohorts, making it the ideal candidate gene to confirm our findings in independent cohorts. In these datasets, stratifying patients with AML into a "*KITLG*-low" group and a "*KITLG*-high" group, based on the 75th percentile expression (to clearly discriminate patients with high levels of expression; Supplementary Fig. S8C) confirmed a significantly better OS (5-years OS 44.0% vs. 0%, $P = 0.017$ in TCGA-LAML; and 39.8% vs. 20.8%, $P = 0.034$ in Bohlander AML; Fig. 7G), confirming findings in the "training" cohort (Fig. 7E).

Taken together, the data support a predictive working model in which inflammatory remodeling of LEPR$^+$ stromal niche cells suppresses normal hematopoiesis (via downregulation of HSPC regulatory factors) but in which leukemia relapse-initiating cells may remain critically dependent on residual levels of stromal niche support (in particular SCF/KITLG-cKIT signaling) for their survival in the context of chemotherapeutic treatment (Supplementary Fig. S9A). Strong inflammation-associated loss of stromal niches may take away this support, resulting in the impediment of leukemia (initiating) cells and reduced risk of relapse (Supplementary Fig. S9B). Alternatively, but not mutually exclusive to this, direct engagement of leukemia-relapse-initiating cells by an activated immune system (driving inflammatory alterations in stromal cells) may explain the association between inflammation and reduced relapse risk in these patients. Future experiments are warranted to test these working models based on our data.

DISCUSSION

Tumor-promoting inflammation is considered an enabling characteristic of tumorigenesis via tumor-promoting effects that immune cells have on neoplastic cells and disease progression (1). The exact mechanisms linking inflammation to oncogenesis, however, remain incompletely understood.

This, to our knowledge, is the first study to examine the predicted interactions between residual tissue-resident stem/progenitor cells versus their neoplastic counterparts within their native niches and immune environment in *human* cancer at cellular resolution. By exploiting insights in the hematopoietic system, in which stem cells and their niches have been defined at near cellular resolution, we provide experimental support for the view that tumor-associated inflammation can result in the remodeling and deterioration of innate stem/progenitor cell niches. This is predicted to result in the loss of their capacity to support residual normal HSPCs with relative resistance of neoplastic cells. Additionally, cytokines (e.g., TGFβ1, IL6, and JAG1) and extracellular matrix components produced by the inflamed niches may directly restrict nonleukemic HSPC growth (66) while promoting leukemic cell progression (17, 67), thus providing a conceptual basis for tissue repression and competitive advantage of neoplastic cells in AML (Supplementary Fig. S9A).

The data provide human disease relevance to concepts previously postulated by experiments in various murine models, in which leukemic cells alter stromal niches in ways that were proposed to inhibit normal hematopoiesis (by suppression of key HSPC factors; ref. 24) or secretion of inhibitory factors (22, 23), but at the same time remain dependent on these niches for their survival under chemotherapeutic conditions (16, 68).

Our human data implicate inflammatory signaling as a key driver of niche deterioration in AML with potential therapeutic significance.

It is important, however, to note that the cellular taxonomies we established do not include all niche cells that constitute the mammalian hematopoietic system. Specifically, ECs and stromal niche subsets with close anatomic relationship to the (trabecular) bone, as identified in the murine bone marrow (24, 69, 70), are likely absent or underrepresented in human BM aspirates. The limited availability of core biopsies (not a universal diagnostic procedure in AML), as well as the low amount of available tissue and heterogeneity (sampling bias) of core biopsies preclude robust analyses of these types of niche cells presently.

The stromal cells we retrieved from human aspirates show transcriptional resemblance to the LEPR$^+$ perivascular stromal HSPC niches identified in mice (5, 71). This subset of stromal cells, thought to largely overlap with so-called CXCL12-abundant reticular (CAR) cells, is considered to be

Figure 6. Inflammatory stromal activation and impaired expression of HSPC factors in AML are variable between genetic subtypes and risk groups. **A,** Differentially expressed gene programs in BMSCs from AML ($n = 62$) in comparison with NBM ($n = 8$) as assessed by Hallmark GSEA. **B,** Differential expression of genes encoding inflammatory cytokines/modulators and HSPC niche markers/factors in BMSCs from AML in comparison with NBM. **, $P_{adj} < 0.01$; ***, $P_{adj} < 0.001$; ****, $P_{adj} < 0.0001$ by the Wald test and adjusted by FDR. TPM, transcripts per million. **C,** Enrichment of gene sets and expression of genes encoding HSPC niche markers/factors in BMSCs from patients with AML related to mutational status. Enrichment scores are calculated using the gene set variation analysis (GSVA) program. **D,** Enrichment of gene sets and expression of HSPC niche markers/factors in BMSCs from patients with AML related to distinct ELN2017 genetic risk categories. Wilcoxon test is applied for statistical analysis. *, $P < 0.05$. ELN, European Leukemia Network.

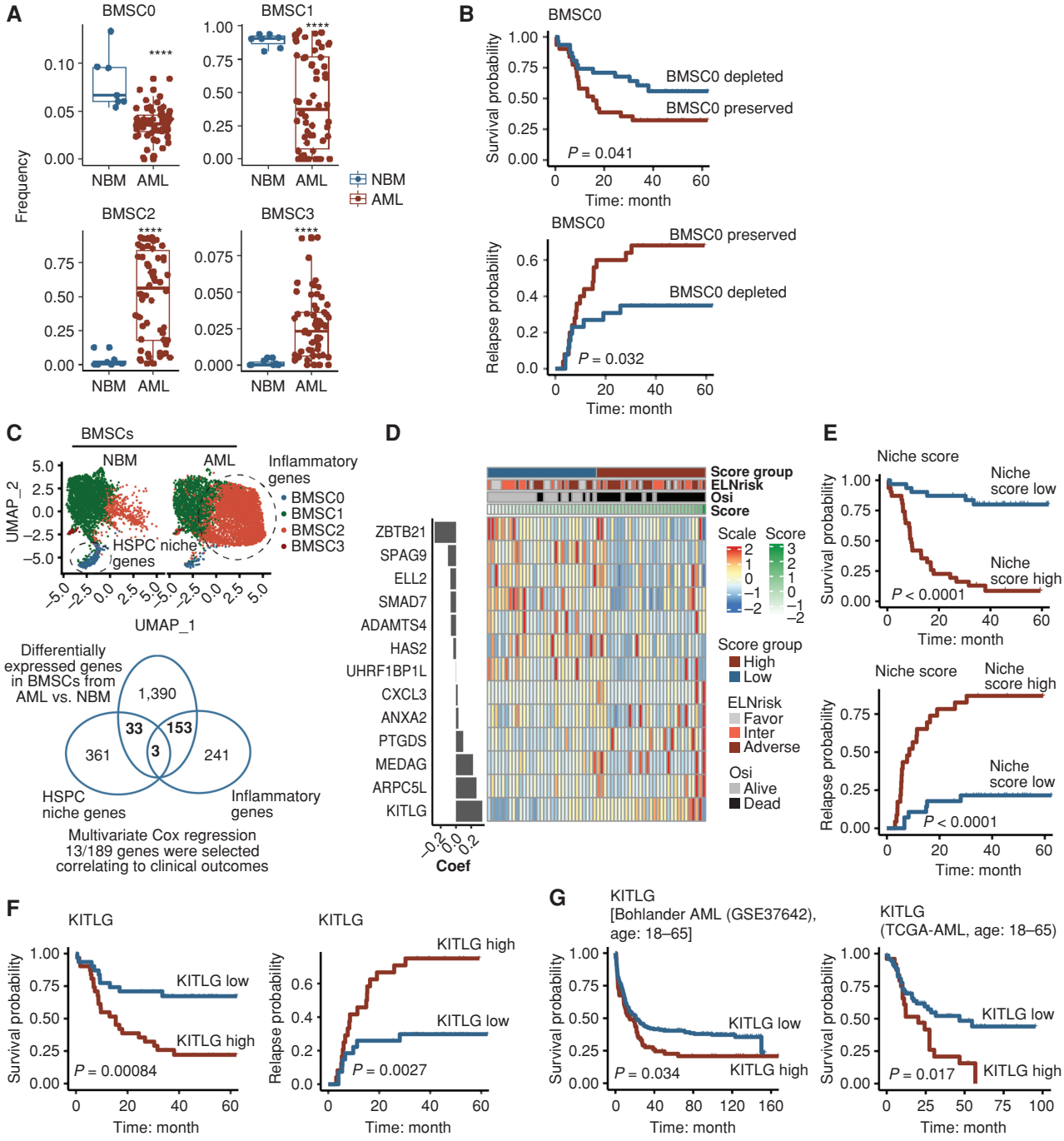

Figure 7. Gene signatures reflective of inflammatory niche remodeling are associated with favorable clinical outcomes in AML. **A,** Predicted BMSC subset size in the larger cohort of patients with AML ($n = 62$). ****, $P < 0.0001$ by the Wilcoxon test. **B,** Kaplan–Meier curves for overall survival (OS) and relapse probability indicating improved outcome in patients with the predicted loss of BMSC cluster 0. Cutoff is median frequency. Statistical significance is determined by a log-rank test. **C,** Construction of a gene signature reflective of niche remodeling (inflammatory activation and relative loss of BMSC cluster 0) in AML. 189 genes at the intersection of the genes differentially expressed in the BMSC-0 vs. other clusters in NBM, the genes differentially expressed in the BMSC-2 vs. other clusters in AML, and the genes differentially expressed in BMSCs in human AML vs. NBM were selected and tested for their correlation with outcome by multivariate Cox regression survival analysis. Thirteen of 189 genes were identified that were associated with outcome. **D,** Coefficient plot (left) and heat map (right) of the 13-gene signature. The gene-expression profile (GEP) score in each patient was calculated using the coefficient and z-scale of the genes. Based on the median GEP score, patients were stratified into two groups, with a high score reflecting relative preservation of niche integrity and a low score reflecting niche inflammatory disruption. **E,** Kaplan–Meier curves for overall survival (OS) and relapse probability indicating improved outcome in patients with niche inflammatory disruption. Cutoff is median score. Log-rank test is used for statistical analysis. **F,** Kaplan–Meier curves OS and relapse probability indicating improved outcome in patients with lower *KITLG* expression in BMSCs. Cutoff is median TPM. Log-rank test is used for statistical analysis. **G,** Kaplan–Meier curves for OS indicating improved outcome in age-matched patients with AML with lower *KITLG* expression in whole BM in Bohlander AML (GSE37642) cohort ($n = 284$) and TCGA-AML cohort ($n = 98$). Cutoff is 75th percentile normalized counts. Log-rank test is used for statistical analysis.

the largest subset of stromal cells in the mammalian BM (2) and has previously been demonstrated to be instrumental for the maintenance of normal HSCs and committed progenitors (72).

In addition to inflammatory remodeling of LEPR$^+$ stromal niches, we describe transcriptional heterogeneity in the human nonleukemic HSC pool and report a previously unanticipated loss of a specific subset of HSCs/MPPs in AML that show strong transcriptional congruence with ST, high-output HSCs previously defined in mice, with relative conservation of LT, low-output HSCs. Due to limitations of 10× scRNA-seq in detecting mutations in genes that are lowly expressed or not near the 3′ end of the transcript (such as *DNMT3A* or *TET2*), we were unable to faithfully discern cells carrying "founder" mutations from truly normal (unmutated) cells in the nonleukemic HSC pool. The data, however, are consistent with the recent finding that residual healthy and preleukemic cells in AML are predominantly dormant (73), and, importantly, put this finding in the context of normal hematopoiesis, revealing a loss of the transcriptional high-output subset of HSCs in AML. These findings may provide not only a cellular basis for the BM failure characterizing AML but also the long-standing observation that normal hematopoiesis is typically reconstituted after chemotherapeutic eradication of leukemic cells, which indicated that a population of cells with HSC characteristics must be able to survive these conditions. Our data indicate that LT-HSCs in the human BM are relatively resistant to inflammatory stress and the loss of SCF from stromal niches, perhaps through the expression of inflammation-inhibiting pathways such as the *NRA* family and *TNFAIP3* (36–38). Other mechanisms likely play a role, and it may be that the transition from LT-HSCs to ST-HSCs is specifically impaired in human AML by yet-to-be-identified factors in the leukemic BM. The identification of transcriptional human HSC subsets and elucidation of the cellular taxonomy of AML reported here is anticipated to enable and facilitate future investigations in these directions.

The nature of the drivers of stromal inflammation remains largely speculative at this point. Our data demonstrate that TNFα, which is commonly overexpressed in myeloid malignancies, is able to induce inflammatory activation and remodeling of the stromal microenvironment. The AML taxonomy indicated that activated immune cells may be a source of TNFα in AML, reminiscent of recent work in mice demonstrating that, in viral infection, activated BM-resident CD8$^+$ T cells induce damage to stromal niches associated with activation of inflammatory pathways and reduction of expression of Cxcl12 and Scf (74). It is, however, reasonable to assume that other sources of TNFα may exist and that multiple inflammatory cytokines are overexpressed in the AML environment that may contribute to stromal remodeling. Future investigations, instructed by the current taxonomies, may shed further light on this. It is further important to note that the negative effects of TNFα on residual normal hematopoiesis in AML are unlikely to be entirely stromal niche-dependent, as TNFα has been demonstrated to exert both positive and negative direct effects on HSPCs (56, 75–78).

Inflammatory remodeling of stromal niches and the associated loss of niche support was associated with a favorable outcome upon chemotherapeutic treatment, supporting the notion that it may pose a therapeutic vulnerability for leukemia-relapse-initiating cells that may remain critically dependent on some residual niche support to ascertain their survival during chemotherapeutic treatment (Supplementary Fig. S9B). Alternatively, or in addition, inflammatory responses driven by activated innate and adaptive immune cells may contribute to the eradication of leukemia-relapse-initiating cells following chemotherapy in niche-independent fashions. This seems consistent with a recent study demonstrating that inflammatory programs in hematopoietic cells result in suppression of adaptive immunity (including T-cell subsets) and poor prognosis (79). Our data indicate that inflammatory activation of stromal niches may be an additional mechanism of T-cell activation-mediated favorable prognosis. Indeed, the observations that *NPM1*-mutated AML is associated with a low (hematopoietic) inflammation score (and associated activation of T cells; ref. 79), but a relatively high stromal inflammation score in our study (relative to "poor risk" genetic subtypes), would be consistent with this. In light of these data, the importance of clearly defining the cellular source and molecular makeup of signatures when using the relatively undescriptive term "inflammation" should be stressed.

The finding that niche signatures associated with clinical outcomes in patients with AML treated with intensive chemotherapy may have an impact on risk stratification and therapeutic decision-making in AML, in which current prediction models are instructed by parameters from hematopoietic cells, rather than their stromal environment (59).

Finally, the presented data are anticipated to provide an important resource of human BM signaling, and in particular stem cell niche interactions, defining normal and leukemic hematopoiesis, to serve as a platform for discovery and validation of findings from nonhuman model systems.

METHODS

Human Normal and AML BM Samples

NBM samples were obtained by hip bone aspiration from healthy donors for allogeneic transplantation.

AML BM aspirates were obtained from newly diagnosed patients with AML (age 18–65) included in the HOVON-132 clinical trial testing the addition of lenalidomide to intensive treatment in younger and middle-aged adults with newly diagnosed AML (57). Patients received two cycles of intensive induction chemotherapy. Cycle 1 included idarubicin at 12 mg/m^2 (3-hour infusion on days 1, 2, and 3) and cytarabine at a dose of 200 mg/m^2 (per continuous infusion on days 1–7) with or without lenalidomide. Cycle 2 contained daunorubicin 60 mg/m^2 per 1-hour infusion on days 1, 3, and 5 plus cytarabine 1,000 mg/m^2 given intravenously for 3 hours twice per day on days 1 to 6 with or without the addition of lenalidomide. Patients in CR or CR with incomplete hematologic recovery (CRi) after cycle 2 received consolidation with 1 final additional cycle of intensive chemotherapy with mitoxantrone–etoposide (cycle 3), autologous stem cell transplantation (auto-SCT), or allogeneic stem cell transplantation (allo-SCT). The study was approved by the ethics committees of the participating institutions and was conducted in accordance with the Declaration of Helsinki. All patients gave their written informed consent (57). BM specimens were collected by hip bone aspiration at diagnosis.

Mononuclear cell fractions of human BM aspirates were isolated using lymphoprep and viably frozen in PBS supplemented with 40% heat-inactivated fetal calf serum (FCS; Corning) and 10% dimethyl

sulfoxide (DMSO; Sigma-Aldrich). Marrow aspirates for scRNA-seq were cryopreserved within 24 hours after collection. All specimens were collected with informed consent, in accordance with the Declaration of Helsinki.

Patient Cell Isolation for RNA-seq

Viably frozen BM aspirates (mononuclear cell fractions) were thawed in a water bath at 37°C and washed with warm Dulbecco's Modified Eagle Medium (DMEM) supplemented with 10% FCS as described in the 10X Genomics protocol "Fresh Frozen Human Peripheral Blood.'

For isolation of hematopoietic fractions, 10% of the thawed BM cells (>20×10^6) from each individual were stained for sorting in PBS supplemented with 0.5% FCS at 4°C with the following antibodies: CD45-APC (1:20, clone 2D1; eBioscience), CD34-AF700 (1:50, clone 581; BioLegend), CD117-PE-CF594 (1:50, clone YB5.B8; BD Biosciences), CD33-PE (1:50, clone P67.6; BD Biosciences), CD3-PE-Cy7 (1:50, clone SK7; BioLegend), CD19-APC-Cy7 (1:50, clone HIB19; BioLegend), and CD38-FITC (1:50, clone HIT2; Life Technologies). For the exclusion of dead cells, 7AAD (1:100; Beckman Coulter) was used. The 7AAD$^-$CD45$^+$CD34$^+$ HSPC fraction, 7AAD$^-$CD45$^+$CD34$^-$CD117$^+$ and 7AAD$^-$CD45$^+$CD34$^-$CD33$^+$ myeloid fraction, and 7AAD$^-$CD45$^+$CD34$^-$CD117$^-$CD33$^-$ nonmyeloid (lymphoid) fraction were sorted in DMEM supplemented with 10% FCS using a FACSAria III (BD Biosciences) and BD FACSDiva version 5.0.

The nonhematopoietic fraction was sorted from the thawed BM cells as described before (80). 90% of the thawed cells (>200×10^6) were stained with biotinylated antibodies against CD45 (1:50, clone HI30; BioLegend) and CD235a (1:50, clone HIR2, BioLegend) followed by depletion using magnetic antibiotin beads (20 μL per 10^7 cells; Miltenyi Biotec) in PBS supplemented with 2% FCS and iMag (BD Biosciences). After depletion, the remaining cells were stained for sorting in PBS containing 0.5% FCS at 4°C with the following antibodies: streptavidin-AF488 (1:100, Invitrogen), CD45-BV510 (1:50, clone HI30; BioLegend), CD235a-PE-Cy7 (1:50, clone HI264; BioLegend), CD71-AF700 (1:20, clone MEM-75; Exbio), CD271-PE (1:50, clone ME20.4; BioLegend), CD105-APC (1:50, clone SN6; eBioscience), CD31-APC-Cy7 (1:20, clone WM59; BioLegend), CD34-eFluor610 (1:50, cone 4H11; eBioscience), and CD144-V450 (1:50, clone 55-7H1; BD Biosciences). 7AAD (1:100; Beckman Coulter) was used for dead cell exclusion. FACSAria III (BD Biosciences) and BD FACSDiva version 5.0 were applied for sorting. 7AAD$^-$CD45$^-$CD235A$^-$CD71$^-$ nonhematopoietic fraction was sorted in DMEM supplemented with 10% FCS for scRNA-seq and 7AAD$^-$CD45$^-$CD235A$^-$CD71$^-$CD31$^-$CD274$^+$ BMSCs were sorted in TRIzol (Life Technologies) for bulk RNA-seq.

scRNA-seq

Prior to scRNA-seq, two fractions sorted separately from the same donors were pooled together (nonhematopoietic fraction with lymphoid fraction and myeloid fraction with HSPC fraction) followed by encapsulation for barcoding and cDNA synthesis using the Chromium Single-cell 3′ Reagent kit v3 (10X Genomics). 3′ gene-expression library was constructed according to the manufacturer's recommendations. The quality and quantity of libraries were determined using an Agilent 2100 Bio-analyzer with 2100 Expert version B.02.11.SI811 software and a High-Sensitivity DNA kit. Libraries were sequenced on a NovaSeq 6000 platform (Illumina), paired-end mode, at a sequencing depth of around 45,000 reads per cell, followed by computational alignment using CellRanger (version 3.0.2, 10X Genomics).

Seurat (R package, version 4.0.0; ref. 81) was used for data preprocessing and downstream analysis. For data preprocessing, datasets were first subjected to quality control steps that included removing doublets (a high ratio of RNA counts vs. feature numbers; >6) and filtering out apoptotic cells determined by the high transcriptional output of mitochondrial genes (>5% of total). Subsequently, single-cell data from separate runs of the same donor were merged to generate a complete picture that includes all cell types for each individual. Aiming at generating a tissue map robustly representing the BM taxonomy in healthy individuals and patients with AML, the merged datasets of each individual were integrated using the integration function in Seurat followed by linear dimensional reduction. That included scaling of gene expression across all cells, principal component analysis on the most variable genes (k = 2,000) and unsupervised clustering using a shared nearest-neighbor modularity optimization-based clustering algorithm (resolution 0.3–1).). To mitigate the effects of cell-cycle heterogeneity, cell-cycle phase scores were calculated based on canonical markers and were regressed as described in the Seurat protocol. The data were visualized using uniform manifold approximation and projection for dimension reduction (UMAP; ref. 82). Cell types were identified by the Clustifyr R package (25) and by reviewing the expression of canonical markers associated with particular cell types. In order to reveal BMSC heterogeneity at a high resolution, BMSCs were separated using the Cellselector function in Seurat and independently preprocessed/analyzed. For HSC analysis, the HSC/MPP population was reclustered in order to study HSC heterogeneity robustly in single samples. Only the samples with >10 cells in the HSC/MPP population were used for the analysis.

Cell trajectory analysis was performed using the Monocle3 R package (https://github.com/cole-trapnell-lab/monocle3). Cellchat and CellphoneDB were applied to predict ligand–receptor interaction between cell types (39, 83). For differential expression gene analysis between samples, a DEseq2 (84)-based *pseuD*E package was developed for the aggregation of single-cell level gene counts and application of differential expression (DE) analysis (software is available at https://github.com/weversMJW/pseude). For GSEA (85) between groups, variable genes were identified using Seurat's Findmarker function and ranked using the formula $-\text{sign}(\log_2\text{foldchange}) \times \log_{10}(P\text{ value})$. The R package fgsea was used for the analysis with a permutation of 1,000 using predefined gene sets from the Molecular Signatures Database (MSigDB 6.2) as input. Gene enrichment scores for individual cells were calculated using Seurat's AddGeneScore function, which calculates the score by counting the average expression levels of provided genes, subtracted by the aggregated expression of randomly selected control genes.

Identification of NPM1m *Cells*

Identification of cells carrying the *NPM1* mutation was performed using an in-house–developed tool. In short, alignment results produced by the Cell Ranger pipeline in the form of a BAM file were used as input. Aligned reads, representing sequenced cDNA molecules, were extracted at the mutation position and screened for the *NPM1* mutation taking into account the cellular barcode (CB) and unique molecular identifier (UMI), irrespective of whether the cell is of hematopoietic origin. Following UMI-based consensus sequence building, mutant-carrying reads were assigned to the cell of origin based on the CB. Reads without direct detection of the *NPM1* mutation, i.e., the known 4-nucleotide insert is absent, were screened by a second approach. The *NPM1* mutation is located close to an intron-exon boundary which can result in improper alignment when the mutation is positioned near the extremities of the cDNA molecule, i.e., the 4-nucleotide insert mutation is partially, abnormally, or not introduced (only missense variants) in the aligned read, which in turn complicates detection of the mutation. To prevent this issue, all reads without detected *NPM1* mutation in the first screening round were aligned to the reference genome (hg38) and a modified version thereof including the 4-nucleotide insert mutation, in both cases taking into account the local *NPM1* splicing pattern (i.e., splicing

from the penultimate to terminal exon). Reads aligning best to the reference genome were labeled wild-type and those aligning better to the modified version were labeled mutant. Using UMI-based consensus building, mutant-carrying and wild-type reads identified in the second round of screening were attributed to cells based on the CB. Subsequent to the two screening rounds, each cell was assigned a number of UMI-controlled wild-type and mutant reads covering the mutation position. Cells with at least one mutant read detected were classified as *NPM1* mutants. Cells with at least three wild-type reads detected covering the mutation position are classified as likely *NPM1* wild-type. All remaining cells that did not pass these criteria were classified as "nonassignable (NA)." Software is available at https://github.com/RemcoHoogenboezem/annotate_bam_statistics_sc.

Bulk RNA-seq

RNA was extracted using TRIzol reagent (Invitrogen) according to the manufacturer's instructions, in combination of isolation with GenElute LPA (Sigma-Aldrich). cDNA was prepared using the SMARTer procedure through the SMART-Seq v4 Ultra Low Input RNA Kit (Clontech) for Illumina Sequencing. Quantity and quality of cDNA production were assessed using the Agilent 2100 Bio-analyzer and the High Sensitivity DNA kit. cDNA libraries were generated using the TruSeq Sample Preparation v2 guide (Illumina) and paired-end sequencing on a NovaSeq 6000 (Illumina). Adaptor sequences and polyT tails were trimmed from unprocessed reads using fqtrim version 0.9.7. (http://ccb.jhu.edu/software/fqtrim/). Read counts and transcripts per million (TPM) were determined with Salmon version 1.2.1 (86). Gene count estimates were determined from Salmon output with the tximport R package version 1.16 (87). These gene count estimates were in turn normalized, prefiltered according to standard practices, and used for determining the differential gene expression between groups of interest through the DESeq2 package (version 1.28; ref. 84) using default parameters. GSEA was performed with GSEA software (version 3.0, Broad Institute) using predefined gene sets from the Molecular Signatures Database (MSigDB 6.2). Gene lists were ranked on the basis of the log2 FC made available through the DESeq2 package. Classic enrichment statistics with 1,000 permutations were used to determine significant enrichment within gene sets. GSVA (R package) was applied for gene enrichment analysis in single samples.

Fluorescence IHC

BM biopsies were fixed in 4% paraformaldehyde, decalcified in 150 mmol/L EDTA, washed in 70% ethanol, and embedded in paraffin. Sections of 5-μm BM biopsies were deparaffinized in xyleen and hydrated in a graded series of ethanol. Antigen retrieval was achieved by microwave treatment in TRIS-EDTA buffer (1M Tris, 0.5M EDTA, 0.05% Tween-20, PH = 9.0). Slides were subsequently blocked using BloxALL (Vector Laboratories), to block endogenous peroxidases, PBS supplemented with 0.5% Tween-20, 5% human serum, 5% goat serum, and 5% donkey serum to circumvent nonspecific binding, and were stained overnight at 4°C with primary antibodies. The primary antibodies that were used in this study included rabbit anti-human CD271 (1:100, HPA004765, BioLegend), mice anti-human CXCL12 (1:50, clone 79018, Invitrogen), and rat anti-human CD44 (1:50, clone IM7, Invitrogen). The secondary antibodies included Alexa Fluor 488–labeled donkey anti-mouse (Invitrogen, 1:200), horseradish peroxidase (HRP)-labeled goat anti–rat (1:100, Jackson ImmunoResearch), and cy5-labeled donkey anti-rabbit antibodies (1:800, Jackson ImmunoResearch). A Tyramide superboost kit (Invitrogen) was used to label CD44 in AF555 following the manufacturer's protocol. The stained sections were mounted in ProLong Diamond containing DAPI (Invitrogen). Images were acquired using a Leica SP5 confocal microscope at 40× magnification and were subsequently analyzed using Fiji software.

Flow Cytometry Analysis for Human BMSCs

Frozen BM aspirates were thawed on ice and stained with biotinylated antibodies against CD45 (1:50, clone HI30; BioLegend) and CD235a (1:50, clone HIR2, BioLegend) followed by depletion using magnetic anti-biotin beads (20 μL per 10^7 cells; Miltenyi Biotec) in PBS supplemented with 2% FCS and iMag (BD Biosciences). After depletion, the remaining cells were stained in PBS containing 0.5% FCS at 4°C with the following antibodies: Streptavidin-AF488 (1:100, Invitrogen), CD45-BV510(1:50, clone HI30; BioLegend), CD235a-PE-Cy7(1:50, clone HI264; BioLegend), CD71-AF700 (1:20, clone MEM-75; Exbio), CD271-PE (1:50, clone ME20.4; BioLegend), CD31-APC-Cy7 (1:20, clone WM59; BioLegend), and CD44-APC (1:50, clone IM7, Sony). 7AAD (1:100; Beckman Coulter) was used for dead cell exclusion. Samples were measured using FACSymphony A5 Cell Analyzer and analyzed with a FlowJo_v10.6.1 program.

Animal Experimental Procedures

Three-month-old C57BL/6 mice were purchased from Charles River and maintained in specific pathogen-free conditions in the Experimental Animal Center of the Erasmus MC (EDC). These mice were intraperitoneally (i.p.) injected with 5 μg recombinant murine TNFα (PeproTech) for 5 consecutive days, followed by peripheral blood collection for complete blood count, and were sacrificed at day 6 by cervical dislocation. For establishment of *MLL-AF9* AML mice model, retroviral plasmid containing MLL-AF9-EGFP (a gift from Dr. Stefan Erkeland, ErasmusMC Rotterdam) were transfected into the platinum-E (Plat-E) retroviral packaging cell line using LipoD293 transfection reagent (SignaGen) for retroviral production. The virus was transduced into freshly isolated Lin^- BM cells derived from 3-month-old B6.SJL mice (from Charles River) after Lin^+ cell depletion using mouse Lineage Cell Depletion Kit (Miltenty Biotec). One million transduced cells (containing ±5% GFP^+ cells) were intravenously injected into lethally irradiated (9.5 Gy) age-matched C57BL/6 mice. When AML had developed (white blood cell counts >15 × 10^3/mm^3) 30 days after injection, mice were sacrificed and BM cells (%GFP^+>90%) were collected. For testing the effects of TNFα on AML, 50,000 BM cells derived from the MLL-AF9 AML mice were intravenously injected into nonirradiated 3-month-old C57BL/L mice. After 30 days of transplantation, 5 μg recombinant murine TNFα (PeproTech) was i.p. injected into the mice for 5 consecutive days, followed by peripheral blood collection for complete blood count. Mice were sacrificed on day 11 (counted from the start date of TNFα injection) by cervical dislocation. Animal studies were approved by the Animal Welfare/Ethics Committee of the EDC in accordance with legislation in the Netherlands (approval No. EMC 2067, 2714, 2892, and 3062).

Flow Cytometry for Mice Bone Fractions and HSPCs

Mice collagenased bone fraction cells were stained with CD45.2-APC-Cy7 (1:200, clone 104, eBiolegend), Ter119-BV510 (1:50, clone TER-119, BioLegend), CD31-PE-Texas-red (1:100, clone MEC13.3, BD Biosciences), CD144-PE-Cy7 (1:200, clone BV13, BioLegend), CD51-PE (1:50, RMV-7, BioLegend), Sca1-PacificBlue (1:100, D7, BioLegend), and LEPR-biotin (1:50, catalog RB01, R&D Systems) followed by staining of streptavidin-APC (1:100, BioLegend) and 7AAD (1:100) in PBS + 0.5% FCS. $7AAD^-CD45.2^-Ter119^-CD31^-CD114^-CD51^+Sac1^-LEPR^+$ and $7AAD^-CD45.2^-Ter119^-CD31^-CD114^-CD51^+Sca1^-LEPR^-$ BMSCs were sorted in TRIzol using FACSAria III (BD Biosciences) and BD FACSDiva version 5.0. Data were analyzed using FlowJo software. For HSPC analysis, mice BM mononuclear cells were first stained with lineage (Lin) cocktail containing biotinylated antibodies against Ly-6G/Ly-6C (Gr-1) Biotin RB6-8C5 (BD Biosciences; 1:100), CD11b Biotin M1/70 (BD Biosciences; 1:100), Ter119 Biotin TER-119 (BD Biosciences; 1:100), CD3e Biotin 145-2C11 (BD

Biosciences; 1:100), CD4 Biotin GK1.5 (BD Biosciences; 1:100), CD8 Biotin 53-6.7 (BD Biosciences; 1:100) and B220 Biotin RA3-6B2 (BD Biosciences; 1:100). After one washing step, cells were incubated with Streptavidin Pacific Orange (Life Technologies; 1:200), together with a combination of the following antibodies: Sca1 Pacific Blue E13-161.7 (BioLegend; 1:100), CD48 AF700 HM48-1 (BioLegend; 1:100), CD150 PE-Cy7 TC15-12F12.2 (BioLegend; 1:100), CD127 (IL7RA) APC A7R34 (BioLegend; 1:100), cKit PE-CF594 2B8 (BD Biosciences; 1:100), CD16/32 APC-Cy7 2.4G2 (BD Biosciences; 1:100), FLT3 APC A2F10 (1:40), and 7-ADD (1:100).

Cell Line and Ex Vivo *Coculture*

The STR-authenticated human BMSC cell line HS-5 was purchased from ATCC (CRL 3611) in 2020 and maintained in RPMI-1640 medium (Thermo Fisher Scientific) supplemented with 10% FCS and 1% penicillin and streptomycin. The cells used in the experiments had passage numbers <12. Mycoplasma testing was performed monthly using a Mycoplasma PCR detection kit (Thermo Fisher Scientific). Primary $CD34^+$ cells were obtained from umbilical cord blood (Erasmus MC) using a Ficoll gradient protocol and by magnetic-activated cell sorting. Primary AML cells were obtained from patients' aspirates as described above. For *ex vivo* coculture, 180,000 HS-5 cells were seeded in each well of a 12-well plate in RPMI-1640 medium supplemented with or without 10 ng/mL recombinant human TNFα (PeproTech). After 24 hours and washing of HS-5 cells with PBS, CB $CD34^+$ cells or primary AML cells were seeded on top of the HS-5 cells and covered with GMP serum-free Stem Cell Growth Medium (CellGenix GmbH) supplemented with 50 ng/mL TPO, 50 ng/mL FLT3, 50 ng/mL SCF, and 20 ng/mL IL3 (only for AML cells; all from PeproTech). Cells were cultured for 3 days at 37°C with 5% CO_2.

Counting of CB $CD34^+$ cells after 3 days of *ex vivo* coculture was accurately obtained with flow-count fluorosphere beads (Beckman Coulter), in combination with the following antibodies: Lin-cocktail-FITC (1:100, catalog 22-7778-72, eBioscience), CD45-APC (1:20, clone 2D1; eBioscience), CD34-AF700 (1:50, clone 581; BioLegend). For counting of AML cells, an antibody cocktail containing CD45-APC (1:20, clone 2D1; eBioscience), CD34-AF700 (1:50, clone 581; BioLegend), CD117-PE-CF594 (1:50, clone YB5.B8; BD Biosciences), CD33-PE (1:50, clone P67.6; BD Biosciences) was used in combination with flow-count fluorosphere beads. In both cases, dead cells were excluded based on the DAPI (1:7,500) gate. The data were acquired using an LSRII flow cytometer (BD Biosciences) and analyzed using FlowJo software.

CFU-GEMM Assay

On day 3 of coculture, 2000 mononuclear cells (MNCs) from HS-5-Veh (PBS) condition and in HS-5-TNFα condition were resuspended in IMDM (Thermo Fisher Scientific). This cell suspension was mixed with MethoCult GF H84434 (STEMCELL Technologies), which allows the growth of colonies from all three lineages, and triplicate dishes were plated. The MethoCult plates were kept at 37°C in a 5% CO_2 incubator for 2 weeks until colony counting under a light microscope (Zeiss).

Survival Analysis

The R package dCVnet (https://github.com/AndrewLawrence/dCVnet) was used to perform Lasso-penalized nested cross-validated Cox regression [k-fold.outer = 5, k-fold.inner = leave-one-out cross-validation (i.e., 1)] to build a predictive model for OS based on the centered and scaled gene expression of the 189 genes from all available AML samples ($n = 62$). This resulted in the retention of 13 out of 189 genes weighted according to their contribution to the model. Similar to Ng and colleagues (61), we obtained a weighted score by taking the linear combination of the centered and scaled gene-expression levels of the 13 retained genes weighted by the obtained regression coefficients. Score = (*ADAMTS4* × –0.066) + (*ZBTB21* × –0.079) + (*HAS2* × –0.035) + (*SPAG9* × –0.104) + (*KITLG* × 0.345) + (*CXCL3* × 0.021) + (*MEDAG* × 0.224) + (*PTGDS* × 0.094) + (*ARPC5L* × 0.269) + (*UHRF1BP1L* × –0.0008) + (*SMAD7* × –0.069) + (ANXA2 × 0032) + (ELL2 × –0.072). The median score value was used to dichotomize the AML cohort into low- and high-score groups. These groups were labeled as "BMSC niche-preserved" (low score) and "BMSC niche inflammatory remodeling" (high score), respectively. Distinction into the "favorable," "intermediate," and "adverse" groups was based on the ELN2017 genetic risk classification. The log-rank test was used to assess statistical differences between the survival distributions, a $P \le 0.05$ was considered statistically significant. For clinical outcome analysis using publicly available datasets, TCGA-LAML and Bohlander AML (GSE37642) datasets were acquired using R package TCGAbiolinks and GEOquery, respectively. Patients between 18 and 65 years old were selected and stratified into KITLG-low and KITLG-high groups based on the 75% percentile of normalized counts of KITLG. The log-rank test was used to assess statistical differences between the survival distributions, a $P \le 0.05$ was considered statistically significant.

Statistical Analysis

Statistical analysis was performed using Prism 8 (GraphPad Software) and/or R program. Unless otherwise specified, unpaired, two-tailed Student *t* test (single test), one-way ANOVA (multiple comparisons), or Spearman rho test (correlation analysis) was used to evaluate statistical significance, defined as *P*-value < 0.05. All results in bar graphs are mean value ± SD.

Data Availability

The RNA-seq data generated in this study were deposited and publicly available in European Genome-Phenome Archive (EGA) at accession number EGAS00001007330. The data analyzed in this study were obtained from the database of Genotypes and Phenotypes (dbGaP) at phs000178 (TCGA-LAML), and Gene-Expression Omnibus at GSE37642. All other data supporting the findings of this study are cited in Methods, in supplementary documents, or are available upon request from the authors.

Authors' Disclosures

No disclosures were reported.

Authors' Contributions

L. Chen: Conceptualization, resources, data curation, software, formal analysis, investigation, visualization, methodology, writing–original draft. **E. Pronk:** Formal analysis, methodology. **C. van Dijk:** Data curation, formal analysis, methodology. **Y. Bian:** Methodology. **J. Feyen:** Methodology. **T. van Tienhoven:** Formal analysis, methodology. **M. Yildirim:** Investigation, methodology. **P. Pisterzi:** Methodology. **M.M. De Jong:** Methodology. **A. Bastidas:** Methodology. **R.M. Hoogenboezem:** Data curation, software, methodology. **C. Wevers:** Software, methodology. **E.M. Bindels:** Data curation, methodology. **B. Löwenberg:** Conceptualization, investigation. **T. Cupedo:** Conceptualization, investigation. **M.A. Sanders:** Conceptualization, investigation, methodology. **M.H.G.P. Raaijmakers:** Conceptualization, supervision, funding acquisition, investigation, writing–original draft, project administration.

Acknowledgments

The authors wish to thank Nathalie Papazian and Michael Vermeulen for technical assistance, Mariette ter Borg for providing $CD34^+$ cells; the HOVON/SAKK leukemia working group and all its members and participating sites for conducting the HOVON132 trial; Peter Valk, Patrycja Gradowska, and Jurjen Versluis for providing the genetic and clinical data; the Josephine Nefkens Precision

Cancer Treatment Program for infrastructural support and members of the Erasmus MC Department of Hematology for providing scientific discussion and members of the Erasmus MC animal core facility EDC for help with animal care. This work was supported by grants from the Dutch Cancer Society (KWF Kankerbestrijding), Amsterdam, the Netherlands (grant EMCR 10488 and 11092 to M.H.G.P. Raaijmakers).

The publication costs of this article were defrayed in part by the payment of publication fees. Therefore, and solely to indicate this fact, this article is hereby marked "advertisement" in accordance with 18 USC section 1734.

Note

Supplementary data for this article are available at Blood Cancer Discovery Online (https://bloodcancerdiscov.aacrjournals.org/).

Received March 23, 2023; revised June 9, 2023; accepted July 14, 2023; published first July 19, 2023.

REFERENCES

1. Hanahan D, Weinberg RA. Hallmarks of cancer: the next generation. Cell 2011;144:646–74.
2. Gomariz A, Helbling PM, Isringhausen S, Suessbier U, Becker A, Boss A, et al. Quantitative spatial analysis of haematopoiesis-regulating stromal cells in the bone marrow microenvironment by 3D microscopy. Nat Commun 2018;9:2532.
3. Kfoury Y, Scadden DT. Mesenchymal cell contributions to the stem cell niche. Cell Stem Cell 2015;16:239–53.
4. Ding L, Morrison SJ. Haematopoietic stem cells and early lymphoid progenitors occupy distinct bone marrow niches. Nature 2013;495:231–5.
5. Ding L, Saunders TL, Enikolopov G, Morrison SJ. Endothelial and perivascular cells maintain haematopoietic stem cells. Nature 2012;481:457–62.
6. Morikawa S, Mabuchi Y, Kubota Y, Nagai Y, Niibe K, Hiratsu E, et al. Prospective identification, isolation, and systemic transplantation of multipotent mesenchymal stem cells in murine bone marrow. J Exp Med 2009;206:2483–96.
7. Omatsu Y, Sugiyama T, Kohara H, Kondoh G, Fujii N, Kohno K, et al. The essential functions of adipo-osteogenic progenitors as the hematopoietic stem and progenitor cell niche. Immunity 2010;33:387–99.
8. Zhou BO, Yue R, Murphy MM, Peyer JG, Morrison SJ. Leptin-receptor-expressing mesenchymal stromal cells represent the main source of bone formed by adult bone marrow. Cell Stem Cell 2014;15:154–68.
9. Comazzetto S, Murphy MM, Berto S, Jeffery E, Zhao Z, Morrison SJ. Restricted hematopoietic progenitors and erythropoiesis require SCF from leptin receptor+ niche cells in the bone marrow. Cell Stem Cell 2019;24:477–86.
10. Kohara H, Omatsu Y, Sugiyama T, Noda M, Fujii N, Nagasawa T. Development of plasmacytoid dendritic cells in bone marrow stromal cell niches requires CXCL12-CXCR4 chemokine signaling. Blood 2007;110:4153–60.
11. Noda M, Omatsu Y, Sugiyama T, Oishi S, Fujii N, Nagasawa T. CXCL12-CXCR4 chemokine signaling is essential for NK-cell development in adult mice. Blood 2011;117:451–8.
12. Tokoyoda K, Hauser AE, Nakayama T, Radbruch A. Organization of immunological memory by bone marrow stroma. Nat Rev Immunol 2010;10:193–200.
13. Abarrategi A, Mian SA, Passaro D, Rouault-Pierre K, Grey W, Bonnet D. Modeling the human bone marrow niche in mice: from host bone marrow engraftment to bioengineering approaches. J Exp Med 2018;215:729–43.
14. Dong L, Yu WM, Zheng H, Loh ML, Bunting ST, Pauly M, et al. Leukaemogenic effects of Ptpn11 activating mutations in the stem cell microenvironment. Nature 2016;539:304–8.
15. Duarte D, Hawkins ED, Akinduro O, Ang H, De Filippo K, Kong IY, et al. Inhibition of endosteal vascular niche remodeling rescues hematopoietic stem cell loss in AML. Cell Stem Cell 2018;22:64–77.
16. Forte D, Garcia-Fernandez M, Sanchez-Aguilera A, Stavropoulou V, Fielding C, Martin-Perez D, et al. Bone marrow mesenchymal stem cells support acute myeloid leukemia bioenergetics and enhance antioxidant defense and escape from chemotherapy. Cell Metab 2020;32:829–43.
17. Kode A, Manavalan JS, Mosialou I, Bhagat G, Rathinam CV, Luo N, et al. Leukaemogenesis induced by an activating beta-catenin mutation in osteoblasts. Nature 2014;506:240–4.
18. Krause DS, Fulzele K, Catic A, Sun CC, Dombkowski D, Hurley MP, et al. Differential regulation of myeloid leukemias by the bone marrow microenvironment. Nat Med 2013;19:1513–7.
19. Raaijmakers MH, Mukherjee S, Guo S, Zhang S, Kobayashi T, Schoonmaker JA, et al. Bone progenitor dysfunction induces myelodysplasia and secondary leukaemia. Nature 2010;464:852–7.
20. Sanchez-Aguilera A, Mendez-Ferrer S. The hematopoietic stem-cell niche in health and leukemia. Cell Mol Life Sci 2017;74:579–90.
21. Schepers K, Pietras EM, Reynaud D, Flach J, Binnewies M, Garg T, et al. Myeloproliferative neoplasia remodels the endosteal bone marrow niche into a self-reinforcing leukemic niche. Cell Stem Cell 2013;13:285–99.
22. Waclawiczek A, Hamilton A, Rouault-Pierre K, Abarrategi A, Albornoz MG, Miraki-Moud F, et al. Mesenchymal niche remodeling impairs hematopoiesis via stanniocalcin 1 in acute myeloid leukemia. J Clin Invest 2020;130:3038–50.
23. Zambetti NA, Ping Z, Chen S, Kenswil KJG, Mylona MA, Sanders MA, et al. Mesenchymal inflammation drives genotoxic stress in hematopoietic stem cells and predicts disease evolution in human preleukemia. Cell Stem Cell 2016;19:613–27.
24. Baryawno N, Przybylski D, Kowalczyk MS, Kfoury Y, Severe N, Gustafsson K, et al. A cellular taxonomy of the bone marrow stroma in homeostasis and leukemia. Cell 2019;177:1915–32.
25. Fu R, Gillen AE, Sheridan RM, Tian C, Daya M, Hao Y, et al. clustifyr: an R package for automated single-cell RNA sequencing cluster classification. F1000Res 2020;9:223.
26. Pellin D, Loperfido M, Baricordi C, Wolock SL, Montepeloso A, Weinberg OK, et al. A comprehensive single-cell transcriptional landscape of human hematopoietic progenitors. Nat Commun 2019;10:2395.
27. Chen L, Kostadima M, Martens JHA, Canu G, Garcia SP, Turro E, et al. Transcriptional diversity during lineage commitment of human blood progenitors. Science 2014;345:1251033.
28. Rodriguez-Fraticelli AE, Weinreb C, Wang SW, Migueles RP, Jankovic M, Usart M, et al. Single-cell lineage tracing unveils a role for TCF15 in haematopoiesis. Nature 2020;583:585–9.
29. Giladi A, Paul F, Herzog Y, Lubling Y, Weiner A, Yofe I, et al. Single-cell characterization of haematopoietic progenitors and their trajectories in homeostasis and perturbed haematopoiesis. Nat Cell Biol 2018;20:836–46.
30. Velten L, Haas SF, Raffel S, Blaszkiewicz S, Islam S, Hennig BP, et al. Human haematopoietic stem cell lineage commitment is a continuous process. Nat Cell Biol 2017;19:271–81.
31. Carrelha J, Meng Y, Kettyle LM, Luis TC, Norfo R, Alcolea V, et al. Hierarchically related lineage-restricted fates of multipotent haematopoietic stem cells. Nature 2018;554:106–11.
32. Sanjuan-Pla A, Macaulay IC, Jensen CT, Woll PS, Luis TC, Mead A, et al. Platelet-biased stem cells reside at the apex of the haematopoietic stem-cell hierarchy. Nature 2013;502:232–6.
33. Laurenti E, Frelin C, Xie S, Ferrari R, Dunant CF, Zandi S, et al. CDK6 levels regulate quiescence exit in human hematopoietic stem cells. Cell Stem Cell 2015;16:302–13.
34. Scheicher R, Hoelbl-Kovacic A, Bellutti F, Tigan AS, Prchal-Murphy M, Heller G, et al. CDK6 as a key regulator of hematopoietic and leukemic stem cell activation. Blood 2015;125:90–101.
35. Li J, Williams MJ, Park HJ, Bastos HP, Wang X, Prins D, et al. STAT1 is essential for HSC function and maintains MHCIIhi stem cells that resist myeloablation and neoplastic expansion. Blood 2022;140:1592–606.

36. Muto T, Walker CS, Choi K, Hueneman K, Smith MA, Gul Z, et al. Adaptive response to inflammation contributes to sustained myelopoiesis and confers a competitive advantage in myelodysplastic syndrome HSCs. Nat Immunol 2020;21:535–45.
37. Freire PR, Conneely OM. NR4A1 and NR4A3 restrict HSC proliferation via reciprocal regulation of C/EBPalpha and inflammatory signaling. Blood 2018;131:1081–93.
38. Avagyan S, Henninger JE, Mannherz WP, Mistry M, Yoon J, Yang S, et al. Resistance to inflammation underlies enhanced fitness in clonal hematopoiesis. Science 2021;374:768–72.
39. Jin S, Guerrero-Juarez CF, Zhang L, Chang I, Ramos R, Kuan CH, et al. Inference and analysis of cell-cell communication using CellChat. Nat Commun 2021;12:1088.
40. Sugiyama T, Kohara H, Noda M, Nagasawa T. Maintenance of the hematopoietic stem cell pool by CXCL12-CXCR4 chemokine signaling in bone marrow stromal cell niches. Immunity 2006;25:977–88.
41. Tokoyoda K, Egawa T, Sugiyama T, Choi BI, Nagasawa T. Cellular niches controlling B lymphocyte behavior within bone marrow during development. Immunity 2004;20:707–18.
42. Wang Y, Szretter KJ, Vermi W, Gilfillan S, Rossini C, Cella M, et al. IL-34 is a tissue-restricted ligand of CSF1R required for the development of Langerhans cells and microglia. Nat Immunol 2012;13:753–60.
43. Kim I, Kim HG, Kim H, Kim HH, Park SK, Uhm CS, et al. Hepatic expression, synthesis and secretion of a novel fibrinogen/angiopoietin-related protein that prevents endothelial-cell apoptosis. Biochem J 2000;346(Pt 3):603–10.
44. Cordeiro Gomes A, Hara T, Lim VY, Herndler-Brandstetter D, Nevius E, Sugiyama T, et al. Hematopoietic stem cell niches produce lineage-instructive signals to control multipotent progenitor differentiation. Immunity 2016;45:1219–31.
45. Soliman H, Theret M, Scott W, Hill L, Underhill TM, Hinz B, et al. Multipotent stromal cells: one name, multiple identities. Cell Stem Cell 2021;28:1690–707.
46. Yue R, Zhou BO, Shimada IS, Zhao Z, Morrison SJ. Leptin receptor promotes adipogenesis and reduces osteogenesis by regulating mesenchymal stromal cells in adult bone marrow. Cell Stem Cell 2016;18:782–96.
47. van Galen P, Hovestadt V, Wadsworth Ii MH, Hughes TK, Griffin GK, Battaglia S, et al. Single-cell RNA-seq reveals AML hierarchies relevant to disease progression and immunity. Cell 2019;176:1265–81.
48. Falini B, Mecucci C, Tiacci E, Alcalay M, Rosati R, Pasqualucci L, et al. Cytoplasmic nucleophosmin in acute myelogenous leukemia with a normal karyotype. N Engl J Med 2005;352:254–66.
49. Spaeth EL, Labaff AM, Toole BP, Klopp A, Andreeff M, Marini FC. Mesenchymal CD44 expression contributes to the acquisition of an activated fibroblast phenotype via TWIST activation in the tumor microenvironment. Cancer Res 2013;73:5347–59.
50. Blume-Jensen P, Janknecht R, Hunter T. The kit receptor promotes cell survival via activation of PI 3-kinase and subsequent Akt-mediated phosphorylation of Bad on Ser136. Curr Biol 1998;8:779–82.
51. Feng LX, Ravindranath N, Dym M. Stem cell factor/c-kit up-regulates cyclin D3 and promotes cell cycle progression via the phosphoinositide 3-kinase/p70 S6 kinase pathway in spermatogonia. J Biol Chem 2000;275:25572–6.
52. Alcalay M, Tiacci E, Bergomas R, Bigerna B, Venturini E, Minardi SP, et al. Acute myeloid leukemia bearing cytoplasmic nucleophosmin (NPMc+ AML) shows a distinct gene expression profile characterized by up-regulation of genes involved in stem-cell maintenance. Blood 2005;106:899–902.
53. Weimar IS, Voermans C, Bourhis JH, Miranda N, van den Berk PC, Nakamura T, et al. Hepatocyte growth factor/scatter factor (HGF/SF) affects proliferation and migration of myeloid leukemic cells. Leukemia 1998;12:1195–203.
54. Stevens AM, Miller JM, Munoz JO, Gaikwad AS, Redell MS. Interleukin-6 levels predict event-free survival in pediatric AML and suggest a mechanism of chemotherapy resistance. Blood Adv 2017;1:1387–97.
55. Sanchez-Correa B, Bergua JM, Campos C, Gayoso I, Arcos MJ, Banas H, et al. Cytokine profiles in acute myeloid leukemia patients at diagnosis: survival is inversely correlated with IL-6 and directly correlated with IL-10 levels. Cytokine 2013;61:885–91.
56. Yamashita M, Passegue E. TNF-alpha coordinates hematopoietic stem cell survival and myeloid regeneration. Cell Stem Cell 2019;25:357–72.
57. Lowenberg B, Pabst T, Maertens J, Gradowska P, Biemond BJ, Spertini O, et al. Addition of lenalidomide to intensive treatment in younger and middle-aged adults with newly diagnosed AML: the HOVON-SAKK-132 trial. Blood Adv 2021;5:1110–21.
58. Hanzelmann S, Castelo R, Guinney J. GSVA: gene set variation analysis for microarray and RNA-seq data. BMC Bioinf 2013;14:7.
59. Dohner H, Estey E, Grimwade D, Amadori S, Appelbaum FR, Buchner T, et al. Diagnosis and management of AML in adults: 2017 ELN recommendations from an international expert panel. Blood 2017;129:424–47.
60. Newman AM, Steen CB, Liu CL, Gentles AJ, Chaudhuri AA, Scherer F, et al. Determining cell type abundance and expression from bulk tissues with digital cytometry. Nat Biotechnol 2019;37:773–82.
61. Ng SW, Mitchell A, Kennedy JA, Chen WC, McLeod J, Ibrahimova N, et al. A 17-gene stemness score for rapid determination of risk in acute leukaemia. Nature 2016;540:433–7.
62. Afrakhte M, Moren A, Jossan S, Itoh S, Sampath K, Westermark B, et al. Induction of inhibitory Smad6 and Smad7 mRNA by TGF-beta family members. Biochem Biophys Res Commun 1998;249:505–11.
63. Bitzer M, von Gersdorff G, Liang D, Dominguez-Rosales A, Beg AA, Rojkind M, et al. A mechanism of suppression of TGF-beta/SMAD signaling by NF-kappa B/RelA. Genes Dev 2000;14:187–97.
64. Cancer Genome Atlas Research N, Ley TJ, Miller C, Ding L, Raphael BJ, Mungall AJ, et al. Genomic and epigenomic landscapes of adult de novo acute myeloid leukemia. N Engl J Med 2013;368:2059–74.
65. Herold T, Jurinovic V, Batcha AMN, Bamopoulos SA, Rothenberg-Thurley M, Ksienzyk B, et al. A 29-gene and cytogenetic score for the prediction of resistance to induction treatment in acute myeloid leukemia. Haematologica 2018;103:456–65.
66. Ohta M, Greenberger JS, Anklesaria P, Bassols A, Massague J. Two forms of transforming growth factor-beta distinguished by multipotential haematopoietic progenitor cells. Nature 1987;329:539–41.
67. Mei Y, Ren K, Liu Y, Ma A, Xia Z, Han X, et al. Bone marrow-confined IL-6 signaling mediates the progression of myelodysplastic syndromes to acute myeloid leukemia. J Clin Invest 2022;132.
68. Agarwal P, Isringhausen S, Li H, Paterson AJ, He J, Gomariz A, et al. Mesenchymal niche-specific expression of Cxcl12 controls quiescence of treatment-resistant leukemia stem cells. Cell Stem Cell 2019;24:769–84.
69. Tikhonova AN, Dolgalev I, Hu H, Sivaraj KK, Hoxha E, Cuesta-Dominguez A, et al. The bone marrow microenvironment at single-cell resolution. Nature 2019;569:222–8.
70. Baccin C, Al-Sabah J, Velten L, Helbling PM, Grunschlager F, Hernandez-Malmierca P, et al. Combined single-cell and spatial transcriptomics reveal the molecular, cellular and spatial bone marrow niche organization. Nat Cell Biol 2020;22:38–48.
71. Christodoulou C, Spencer JA, Yeh SA, Turcotte R, Kokkaliaris KD, Panero R, et al. Live-animal imaging of native haematopoietic stem and progenitor cells. Nature 2020;578:278–83.
72. Comazzetto S, Shen B, Morrison SJ. Niches that regulate stem cells and hematopoiesis in adult bone marrow. Dev Cell 2021;56:1848–60.
73. Beneyto-Calabuig S, Merbach AK, Kniffka JA, Antes M, Szu-Tu C, Rohde C, et al. Clonally resolved single-cell multi-omics identifies routes of cellular differentiation in acute myeloid leukemia. Cell Stem Cell 2023;30:706–21.
74. Isringhausen S, Mun Y, Kovtonyuk L, Krautler NJ, Suessbier U, Gomariz A, et al. Chronic viral infections persistently alter marrow stroma and impair hematopoietic stem cell fitness. J Exp Med 2021;218:e20192070.
75. Pearl-Yafe M, Mizrahi K, Stein J, Yolcu ES, Kaplan O, Shirwan H, et al. Tumor necrosis factor receptors support murine hematopoietic progenitor function in the early stages of engraftment. Stem Cells 2010;28:1270–80.
76. Pronk CJ, Veiby OP, Bryder D, Jacobsen SE. Tumor necrosis factor restricts hematopoietic stem cell activity in mice: involvement of two distinct receptors. J Exp Med 2011;208:1563–70.

77. Ishida T, Suzuki S, Lai CY, Yamazaki S, Kakuta S, Iwakura Y, et al. Pre-transplantation blockade of TNF-alpha-mediated oxygen species accumulation protects hematopoietic stem cells. Stem Cells 2017;35:989–1002.
78. Meacham CE, Jeffery EC, Burgess RJ, Sivakumar CD, Arora MA, Stanley AM, et al. Adiponectin receptors sustain haematopoietic stem cells throughout adulthood by protecting them from inflammation. Nat Cell Biol 2022;24:697–707.
79. Lasry A, Nadorp B, Fornerod M, Nicolet D, Wu H, Walker CJ, et al. An inflammatory state remodels the immune microenvironment and improves risk stratification in acute myeloid leukemia. Nat Cancer 2023;4:27–42.
80. de Jong MME, Kellermayer Z, Papazian N, Tahri S, Hofste Op Bruinink D, Hoogenboezem R, et al. The multiple myeloma microenvironment is defined by an inflammatory stromal cell landscape. Nat Immunol 2021;22:769–80.
81. Stuart T, Butler A, Hoffman P, Hafemeister C, Papalexi E, Mauck WM 3rd, et al. Comprehensive integration of single-cell data. Cell 2019;177:1888–902.
82. Becht E, McInnes L, Healy J, Dutertre CA, Kwok IWH, Ng LG, et al. Dimensionality reduction for visualizing single-cell data using UMAP. Nat Biotechnol 2018;37:38–44.
83. Efremova M, Vento-Tormo M, Teichmann SA, Vento-Tormo R. CellPhoneDB: inferring cell-cell communication from combined expression of multi-subunit ligand–receptor complexes. Nat Protoc 2020;15:1484–506.
84. Love MI, Huber W, Anders S. Moderated estimation of fold change and dispersion for RNA-seq data with DESeq2. Genome Biol 2014;15:550.
85. Subramanian A, Tamayo P, Mootha VK, Mukherjee S, Ebert BL, Gillette MA, et al. Gene set enrichment analysis: a knowledge-based approach for interpreting genome-wide expression profiles. Proc Natl Acad Sci U S A 2005;102:15545–50.
86. Patro R, Duggal G, Love MI, Irizarry RA, Kingsford C. Salmon provides fast and bias-aware quantification of transcript expression. Nat Methods 2017;14:417–9.
87. Soneson C, Love MI, Robinson MD. Differential analyses for RNA-seq: transcript-level estimates improve gene-level inferences. F1000Res 2015;4:1521.